CERN-LPCC-2022-06
FERMILAB-TM-2779-V
7th July 2022

Towards a combination of LHC and TeVatron *W*-boson mass measurements

The LHC–TeVatron *W*-boson mass combination working group[1]

In this note methodological and modelling considerations towards a combination of the ATLAS, CDF and D0 measurements of the *W*-boson mass are discussed. As they were performed at different moments in time, each measurement employed different assumptions for the modelling of *W*-boson production and decay, as well as different fits of the parton distribution functions of the proton (PDFs). Methods are presented to accurately evaluate the effect of PDFs and other modelling variations on existing measurements, allowing to extrapolate them to any PDF set and to evaluate the corresponding uncertainties. Based on this approach, the measurements can be corrected to a common modelling reference and to the same PDFs, and subsequently combined accounting for PDF correlations in a quantitative way.

[1] More information can be found at:
https://twiki.cern.ch/twiki/bin/view/LHCPhysics/MWCOMB

Contents

1 Introduction **3**

2 Event generation **5**

3 Correlated and uncorrelated sources of uncertainty **6**
3.1 Electroweak corrections 6
3.2 W-boson p_{T} distribution 7
3.3 Spin correlations 8
3.4 PDF uncertainties 9

4 General methodology **9**

5 Measurement emulation **11**
5.1 Event selections, fit ranges and measurement categories 11
5.2 Parameterisation of the CDF experimental resolutions 12
5.3 Parameterisation of the D0 experimental resolutions 13
5.4 Parameterisation of the ATLAS experimental resolutions 16
5.5 Recoil resolution comparisons 17

6 QCD modelling aspects **18**
6.1 Invariant mass and rapidity distribution in RESBOS1 18
6.2 Treatment of spin correlations in W-boson decays 20
6.3 Impact on the final state distributions 22
6.4 Spin correlation effects : summary 29

7 PDF extrapolations **32**
7.1 Updating existing measurements to alternate PDFs 32
7.2 PDF uncertainties 33

8 Comparison of PDF predictions with global Drell-Yan data **33**

9 Conclusion **42**

10 Acknowledgements **43**

1 Introduction

The present note describes several methodological and modelling aspects of an ongoing effort towards a combination of the CDF [1], D0 [2, 3] and ATLAS [4] measurements of the W-boson mass, m_W[2].

At hadron colliders, measurements of m_W rely on the interpretation of the kinematic peaks in leptonic decays. The final-state distributions carry information about the decaying particle mass, but also reflect the W-boson production and decay distributions, in particular the rapidity and transverse momentum distributions, and polarization effects. Predictions are generally obtained using Monte Carlo (MC) event generators and parton distribution functions (PDFs).

The theoretical description of W-boson production and decay is thus of the utmost importance for m_W determinations. The production of W-bosons is now known to next-to-leading order (NLO) in the electroweak coupling α [6] and to the third order in the strong coupling α_S [7, 8]. The NLO mixed $O(\alpha_s\alpha)$ corrections to W production have also recently been calculated [9–12]. A calculation of polarization effects at $O(\alpha_s^2\alpha)$ has appeared in Ref. [13]. Progress has also been made in the determination of the PDFs, with the inclusion of more and more precise data from different colliders and significant methodological improvements [14–16]. The TeVatron and LHC measurements discussed here use different tools for the theoretical description of W-boson production and decay that generally reflect the state of the art at the time they were initiated.

The CDF Collaboration measured m_W [1] using data corresponding to 8.8 fb^{-1} of integrated luminosity collected in proton-antiproton, $p\bar{p}$, collisions at a center-of-mass energy of $\sqrt{s}$ = 1.96 TeV at the TeVatron collider. The mass was obtained with template fits to the reconstructed distributions of the charged lepton transverse momentum, p_T^l, the W-boson transverse mass, m_T^W, and the neutrino transverse momentum, p_T^ν, in the electron and muon decay channels, obtaining m_W = 80433.5 ± 6.4 (stat.) ± 6.9 (sys.) = 80433.5 ± 9.4 MeV. The central value of m_W in CDF was determined using the NNPDF31 PDF set with the PDF uncertainty estimated using the largest 25 symmetric eigenvectors constructed through a principal-component analysis from the full replica set[3]. The central value determination relies on events from the ResBos C [19] generator tuned to fit the Z-boson transverse momentum and with PDF uncertainties estimated using a p_T^W modeled in Pythia6 [20].

The D0 Collaboration performed a measurement of m_W [3] using 4.3 fb^{-1} of integrated luminosity collected in $p\bar{p}$ collisions at $\sqrt{s}$ = 1.96 TeV during Run II of the TeVatron collider. Template fits are performed in the p_T^l, m_T^W and p_T^ν kinematic distributions in the electron decay channel. This result is combined with an earlier D0 result [2] using 1 fb^{-1} of integrated luminosity, yielding m_W = 80375 ± 13 (stat.) ± 22 (sys.) = 80375 ± 23 MeV. The central value of m_W in D0 is determined using the CTEQ6.6 PDF set [21] with uncertainties determined using the CTEQ6.1 PDF rescaling the Hessian eigenvectors to bring the nominal 90% CL coverage to 68% CL. The p_T^W modeling relies on ResBos CP [22, 23] tuned to fit the Z-boson p_T spectrum in data for the determination of the central value, and on Pythia6 for the evaluation of the PDF uncertainties.

The ATLAS Collaboration performed a measurement of m_W using proton-proton, pp, collision data collected at the LHC collider in 2011 at $\sqrt{s}$ = 7 TeV, corresponding to 4.6 fb^{-1} of integrated luminosity. The p_T^l and m_T^W distributions in the electron and muon decay channels are used, giving a result of

[2] The recent LHCB measurement of m_W [5] is expected to be included in the combination at a later stage.

[3] We note that the 2.2 fb^{-1} CDF measurement [17, 18] used the CTEQ6M PDF set with PDF uncertainty estimated using the MSTW2008nnlo set at 68%CL. CTEQ6.6 is quoted in the paper, but the result was actually performed using CTEQ6M.

$m_W = 80370 \pm 7$ (stat.) ± 18 (sys.) $= 80370 \pm 19$ MeV. The ATLAS central value of m_W and its uncertainty are determined with the CT10nnlo PDF set with uncertainties scaled to 68% CL. The p_T^W modeling in ATLAS relies on a parton shower MC Pythia8 [24] tuned to match the p_T^Z in data. The PDF uncertainties are propagated through the rapidity distributions, spin correlations, and their effect on the p_T^W / p_T^Z ratio.

Combining the ATLAS, CDF and D0 results involves three steps: first, the results have to be translated to a common reference model, *i.e.* a common model for the boson rapidity and a common set of proton PDFs; secondly, the correlation of PDF uncertainties at the TeVatron and LHC needs to be evaluated– while both machines are hadron colliders, the different center-of-mass energies (1.96 TeV and 7 TeV for the TeVatron and LHC measurements, respectively) and initial states ($p\bar{p}$ vs. pp) makes this correlation non-trivial; finally, the model dependence of the result is evaluated by repeating this procedure for a relevant set of current PDF sets.

A proper evaluation of PDF uncertainties and their correlations is numerically relevant, as PDFs constitute a dominant source of uncertainty for all measurements. While significant in size, uncertainties related to the p_{T}^W distribution are evaluated separately in each experiment through a detailed analysis of Z-boson production *in situ*, reducing correlations across experiments. Experimental uncertainties are expected to be uncorrelated between experiments.

Beyond the interest of improving the overall measurement precision, several arguments motivate this project :

- At least three averages not endorsed by the TeVatron and LHC collaborations and without explicit estimate of the correlations are being used in recent literature [25–27]. While these numbers may be numerically close to the actual result, they do not rely on an explicitly reproducible methodology that can be used for future averages of this or other hadron collider parameters, and neglect the fact that the measurements were performed with different PDF sets;
- the techniques developed to translate published measurements to a common reference model can also be used to update measurements, *i.e.* to newer, more precise PDF sets or to a better modelling of W-boson production and decay in Quantum Chromodynamics (QCD);
- PDF uncertainty correlations, discussed here for the first time in the context of electroweak precision measurements, will also matter in the joint interpretation of different parameters in electroweak or EFT fits. For example, strong PDF uncertainty correlations are expected between m_W and the effective weak mixing angle, $\sin^2\theta_{\mathrm{eff}}$, when the LHC ultimately dominates the measurement precision for these parameters [28].

The event generators and event samples used for the present analysis are described in Section 2. A general discussion of uncertainty correlations in m_W measurements is first given in Section 3. Section 4 describes the methodology developed for the present analysis, and analysis details are described in Section 5. Updates of the existing measurements for improved predictions are discussed in Section 6, and extrapolations to recent PDF sets are described in Section 7. A comparison of predictions for different PDF sets with Tevatron and LHC Drell-Yan data is given in Section 8, guiding the choice of PDF sets used for the final results. Finally, conclusions are given in Section 9.

2 Event generation

To evaluate the effects of different PDF uncertainties and their correlations, event samples from Monte Carlo event generators are used. $W \to \ell\nu$ and $Z \to \ell\ell$ events are generated for pp collisions at $\sqrt{s} = 7$ TeV and for $p\bar{p}$ collisions at $\sqrt{s} = 1.96$ TeV using different programs.

We consider a wide variety of PDF sets in this combination exercise. These include the PDFs used in the original measurements, either for their central values or to estimate PDF uncertainties, and recent global PDF determinations at NNLO accuracy. The PDFs included are CTEQ6M [29], CTEQ6.1 [30], CTEQ6.6 [21], CT10 [31], CT10nnlo [32], CT14nnlo [33], CT18NNLO and CT18ANNLO [34], MSTW2008nlo with both the 68% CL and 90% CL error sets [35], MMHT2014nnlo68cl [36], MSHT2020nnlo_as118 [15], NNPDF31_nnlo_as_0118 [37], NNPDF40_nnlo_as_01180 [16], ABMP16_5_nnlo [38] and CJ15nlo [39].

In all samples described below, the effect of final-state QED radiation (QED FSR) is included by interfacing the events to Photos-v3.61 [40]. Apart from the collinear photon radiation, which are largely absorbed by "dressing" the leptons with all QED FSR photons within a cone of $\Delta R < 0.1$ around the final state lepton, the generated electron and muon decays are almost identical. Only muons decays are generated and later used for emulating either lepton channel.

A first set of event samples was generated using the W_ew-BMNNP [41] and Z_ew-BMNNPV [42] processes in Powheg-Box-V2 [43–45]. They include Matrix Elements (ME) at next-to-leading order in QCD with renormalization and factorization scales set to the invariant mass of the dilepton system. The nominal event generation is performed with the CT10 PDF set [31], and with $m_W = 80.399$ GeV and $\Gamma_W = 2.085$ GeV. Weights are calculated internally by Powheg that allow the samples to be reweighted to several alternate PDF sets including their eigenvectors or replicas. For each of the nominal PDF sets, large event samples in excess of 0.5×10^9 were also generated directly with those PDF sets to study the accuracy of the reweighting. Since only the four-vectors of leptons ($\ell^{\pm}$, ν) at bare and dressed QED level are required, the analysis is performed at the Les Houches Event level, without interfacing to a parton shower, allowing for an efficient and fast processing with minimal loss of accuracy.

A second set of samples was produced using the Wj-MiNNLO$_{PS}$ event generator [46, 47] in POWHEG-BOX-V2. The MiNNLO$_{PS}$ approach achieves next-to-next-to-leading-order accuracy in the Born process, allowing to estimate the effect of higher-order QCD corrections in the PDF dependence of final state observables. The G_μ EW scheme was used with input parameters $G_F = 1.6639 \times 10^{-5}$ GeV^{-2}, $m_W = 80.385$ GeV, $\Gamma_W = 2.0854$ GeV, $m_Z = 91.187$ GeV, $\Gamma_Z = 2.4952$ GeV, and $m_H = 125$ GeV. The renormalization scale for the two powers of the strong coupling constant is set to $\mu_R = \mu_F = m_{\ell\nu}$, while at large p_{T} the scale used for the NLO W+jet fixed-order piece were set to $\mu_R = \mu_F = p_{\mathrm{T}}$. The value of Q_0, the non-perturbative scale used to regularise the Landau singularity, was set to $Q_0 = 0.0$ GeV. The generation used the NNPDF31_nnlo_as_0118 PDF set, with event weights added for the other PDF sets considered in this study. Samples of 50×10^6 W^+ and W^- Les Houches events for $p\bar{p}$ collisions at $\sqrt{s} = 1.96$ TeV and pp collisions at 7 TeV were produced.

Finally, large event samples of typically 2×10^9 events each were produced using different versions of the ResBos generator, that was used for the m_W measurements performed at the TeVatron. The ResBos event samples come in three flavours:

- a sample of W^+ events, similar to the samples used for the CDF W-mass measurement [1]. The sample is at NLO+NLL accuracy in QCD ("y" grids), uses the "221" set of non-perturbative

parameters to describe the small boson transverse momentum region, and the CTEQ6M PDF set. It was generated with the "ResBos-C" [22] code, using $m_W = 80.450$ GeV and $\Gamma_W = 2.120$ GeV;

- samples of W^+ events, similar to the samples used in the D0 W-mass measurement [3]. The grids were generated at NNLO+NNLL accuracy in QCD ("y_k" grids), using the CTEQ6.6 PDF set, and the "321" set of non-perturbative parameters to describe the small boson transverse momentum region. The generation used the "ResBos-CP" [23] code, with $m_W = 80.419$ GeV and $\Gamma_W = 2.071$ GeV;
- samples of W^+ events produced from newly generated ResBos grids provided by the authors [48]. Grids were generated at both NLO+NLL ("y"grids) and NNLO+NNLL accuracy ("y_k" grids) for the different PDF sets considered in this study. The generation used a version of ResBos provided by the authors [23], and set $m_W = 80.378$ GeVand $\Gamma_W = 2.0458$ GeV. These newly provided grids contain improvements in the theoretical description of W production and decay, which are further discussed in Ref. [49, 50], and are to be considered an improvement over the predictions used in the original CDF and D0 W-mass measurements.

Throughout this note, the ResBos versions used by CDF and D0 will be referred to as ResBos1, while the new samples will be referred to as ResBos2. All samples can be transformed to common baseline values for m_W and Γ_W, using event weights as described in Section 4.

Comparing the Resbos2 samples to the legacy samples used by CDF and D0 allows to evaluate the shift in m_W corresponding to the theoretical improvements, and enables a consistent theoretical description for all measurements. A comparison of Powheg, MiNNLO, and the new ResBos2 grids will allow to test for model and generator dependencies in the PDF extrapolations in a future update.

3 Correlated and uncorrelated sources of uncertainty

Experimental uncertainties are treated as uncorrelated across experiments. Modelling uncertainties can be categorized as induced by the PDFs, by the p_{T}^W distributions or by electroweak corrections and are discussed below.

3.1 Electroweak corrections

The dominant electroweak effect on the W boson mass measurement originates from the reduction of the measured lepton momentum due to final-state QED radiation. The experiments model this radiation with the PHOTOS generator, that resums multiple soft photon emissions above an energy threshold. Uncertainties on the modelling of electroweak corrections include: (1) the difference between the shower model and an explicit matrix-element calculation; (2) the energy threshold for producing final-state photons; and (3) higher-order corrections from final-state e^+e^- pair production. Tables 1 and 2 list the size of these uncertainties for each experiment in the electron and muon channels, respectively. The uncertainties are completely correlated between the channels.

To estimate the uncertainty from the limitations of the shower model relative to the matrix-element calculation, D0 performs a direct comparison between PHOTOS and WGRAD [51, 52]. ATLAS estimates the uncertainty with a similar procedure but with WINHAC [53–55] providing the NLO model. CDF uses a different strategy, applying a correction to the measurement using the HORACE [56–58] generator,

Uncertainty	CDF	D0	ATLAS	CDF-ATLAS	CDF-D0	D0-ATLAS
NLO calculation	4 (4)	5 (5)	2.5 (3.3)	0%	0%	0%
Photon y cutoff	2 (2)	2 (1)	−−	−−	100%	−−
FSR e^+e^-	1 (1)	−−	0.8 (3.6)	0%	−−	−−
Total	4 (4)	7 (7)	2.6 (4.9)			

Table 1: QED uncertainties in MeV on the m_W measurement in the electron channel using the m_T (p_T) fit. Uncertainty correlations between each pair of experiments are shown.

Uncertainty	CDF	ATLAS
NLO calculation	4 (4)	2.5 (3.5)
Photon y cutoff	2 (2)	−−
FSR e^+e^-	1 (1)	0.8 (3.6)
Total	4 (4)	2.6 (5.6)

Table 2: QED uncertainties in MeV on the m_W measurement in the muon channel using the m_T (p_T) fit. The uncertainties are uncorrelated between the experiments.

which matches multiple-photon radiation to the $O(\alpha)$ calculation. The residual uncertainties are largely due to MC statistics, and are thus considered as uncorrelated.

The shower model includes the effect of a lower threshold on the emitted photon energy, expressed as a ratio y with respect to the energy of the lepton from the W boson decay. CDF uses a threshold of 10^{-5} and determines the uncertainty by increasing the threshold by an order of magnitude. D0 uses a similar procedure except with an increase from 2.5×10^{-4} to 2×10^{-2} in y. These uncertainties are taken to be completely correlated.

To account for the higher-order process of an off-shell final-state photon splitting into an e^+e^- pair, CDF applies an effective radiator approximation to the radiated photons. ATLAS does not apply a correction, instead taking the uncertainty from a PHOTOS model of this process. The uncertainties are treated as uncorrelated.

3.2 W-boson p_{T} distribution

The prediction of the W-boson p_{T} distribution is a second potential source of uncertainty correlation. In the region relevant for m_W, the p_{T} distribution is described by a combination of perturbative fixed-order QCD, soft-gluon resummation and non-perturbative effects. The TeVatron experiments use analytical resummation as implemented in ResBos1, while ATLAS rely on the Pythia8 parton shower.

Non-perturbative effects influence the very low boson p_{T}^W region, typically $p_{\mathrm{T}}^W < 5$ GeV and are generally assumed to be universal between W and Z production. In absence of precise direct measurements of the W-boson p_{T} distribution, all measurements rely on Z-boson data to constrain the corresponding parameters.

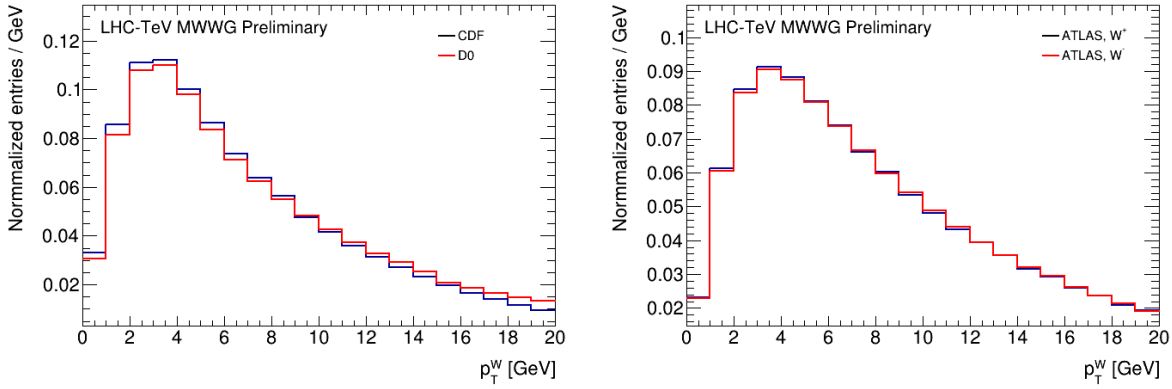

Figure 1: Baseline transverse-momentum distributions for selected $W^{\pm}$ events in CDF and D0 (left), in $p\bar{p}$ collisions at 1.96 TeV, and for W^+ and W^- events from 7 TeV pp collisions in ATLAS. The distributions represent the best-fit model resulting from the analysis of Z-boson data in the respective experiments, and are shown after all event selections.

The resulting model is then used for the prediction of the W-boson p_{T} distribution. The associated uncertainty originates from the limited precision of the Z-boson data, and from differences between the Z and W production mechanisms, in particular related to the different initial-state partonic configurations.

ATLAS, CDF, and D0 derive the W-boson p_{T}^W distribution from their respective Z-boson data; ATLAS tuned the shower and non-perturbative parameters in Pythia, while CDF and D0 use fits to the non-perturbative resummation parameters g_1, g_2 in ResBos1 for this modelling aspect. The resulting p_{T}^W distributions, after analysis cuts using the emulations discussed in Section 5, are shown in Figure 1. Theoretical uncertainties in the extrapolation from the p_{T}^Z distribution to the p_{T}^W distribution are considered by the ATLAS and CDF experiments, which use the observed W p_{T} distribution to validate (ATLAS) or further constrain (CDF) the associated uncertainty in situ. Once propagated to the W mass measurement, CDF quotes an uncertainty on the W p_{T} modelling of 2.2 MeV, D0 of 2.4 MeV. ATLAS quotes 6.0 MeV, including parton-shower tuning uncertainties and uncertainties in the ratio of the W and Z p_{T} distributions under model variations. Uncertainties related to the W-boson p_{T} distribution can thus be considered as uncorrelated between the three experiments.

3.3 Spin correlations

The theoretical predictions of the lepton p_{T} and transverse mass distributions are affected by the description of the W-boson polarization states. A general expression for the fully differential W-boson production and decay distributions, true at all orders in QCD, is

$$\begin{aligned}\frac{d\sigma}{d\Omega} = \frac{d\sigma}{dm dp_{\mathrm{T}} dy}\,[\; &(1+\cos^2\theta) \\ &+ \frac{1}{2}A_0(1-3\cos^2\theta) + A_1 \sin 2\theta\cos\phi \\ &+ \frac{1}{2}A_2 \sin^2\theta\cos 2\phi + A_3 \sin\theta\cos\phi \\ &+ A_4\cos\theta + A_5\sin^2\theta\sin 2\phi \\ &+ A_6 \sin 2\theta\sin\phi + A_7\sin\theta\sin\phi\;]\,, \end{aligned} \tag{1}$$

where the decay angles θ, ϕ are for example expressed in the Collins-Soper frame [59], and the A_i coefficients generally depend on the W-boson p_{T} and rapidity.

The measurements considered here use theoretical predictions at $O(\alpha_S)$ using ResBos1 for CDF, $O(\alpha_S^2)$ using ResBos1 for D0, and $O(\alpha_S^2)$ using DYNNLO [60, 61] for ATLAS. Only ATLAS considers a systematic uncertainty (5.8 MeV) associated to these predictions, so this effect is not a source of correlation.

In the ResBos1 codes used for the CDF and D0 predictions, the resummation and fixed-order matching affects the distribution of the angular coefficients giving predictions that deviate from the fixed-order calculations. Extrapolated to LHC energies the predictions are expected to also significantly deviate from measurements [62]. This behavior has been corrected ResBos2, allowing to reproduce the fixed-order behavior of the angular coeffficients. This version is believed to be more accurate and motivates an update of the CDF and D0 measurements, which is further discussed in Section 6.2.

3.4 PDF uncertainties

PDF uncertainties constitute the main source of correlation between the measurements. They amount to 3.9 MeV for the CDF measurement (NNPDF3.1), 11 MeV for the D0 measurement (CTEQ6.6), and 9.2 MeV for the ATLAS measurement (CT10nnlo). In the case of the previous Tevatron combination [63], the very similar measurement conditions implied a full correlation of the PDF uncertainty, considered as a single nuisance parameter; differences between the CTEQ6M and CTEQ6.6 PDF sets were neglected. An adapted treatment is being implemented for the present effort.

In contrast, the large gap in energy between the Tevatron and the LHC, as well the different initial states, are expected to induce only a partial correlation of these uncertainties, and a detailed study of the PDF uncertainty components is required. Methods to estimate this correlation are described in Section 4.

4 General methodology

The proposed method relies on an emulation of the existing measurements. The emulation consists of simplified parameterizations of the responses of the experiments, and a reproduction of the corresponding analyses (event selections, fitting procedure, etc). While this approach does not allow an actual measurement, it is adequate for a reliable evaluation of variations in the underlying generator-level distributions, such as PDF uncertainties and extrapolations, and effects in the lepton angular distributions. These effects are calculated as differences or ratios obtained using the same emulation procedure, so that resolution and response effects cancel in first order. The emulation of the ATLAS, CDF and D0 measurements and the associated uncertainties are described in Section 5. This emulation is applied to particle-level W-event samples that reproduce the production and decay distributions expected from different generators or PDFs.

The Monte Carlo samples are produced using reference values for the W-boson mass and width. Kinematic distributions for different values of m_W are obtained by applying the following event weight:

$$w(m, m_W, m_W^{\mathrm{ref}}) = \frac{(m^2 - m_W^2)^2 + m^4\Gamma_w^2/m_W^2}{(m^2 - m_W^{\mathrm{ref}\,2})^2 + m^4\Gamma_w^2/m_W^{\mathrm{ref}\,2}} \tag{2}$$

which represents the ratio of the Breit–Wigner densities corresponding to m_W and $m_W^{\rm ref}$, for a given value of the final state invariant mass m. The present parameterisation uses the running width scheme, in accordance with the published measurement procedures.

The shift in the measured value of m_W resulting from a change in the generator distributions is estimated at the detector level. Considering a set of template distributions obtained for different values of m_W and a given reference prediction, and "pseudo-data" distributions obtained for $m_W = m_W^{\rm ref}$ and an alternate prediction, the preferred value of m_W for the alternate prediction is determined by minimizing the χ^2 between the pseudo-data and the templates. The corresponding shift is defined as $\delta m_W = m_W^{\rm fit} - m_W^{\rm ref}$.

The quality of the boson mass reweighting has been evaluated in a closure test comparing the final-state distributions of $m_{\rm T}$, $p_{\rm T}^{\ell}$ and $p_{\rm T}^{\nu}$ for a reference sample and independent samples generated using different values of m_W and Γ_W. The reweighting is found to close within $\delta m_W < 0.2$ MeV, below the statistical precision of the test.

The shifts are used to re-interpret existing measurements for improved generator predictions, alternate PDF sets and to estimate the corresponding PDF uncertainty. The full correction procedure can be written as follows:

$$m_W^{\rm updated} = m_W^{\rm ref} - \delta m_W^{\rm QCD} - \delta m_W^{\rm PDF} \tag{3}$$

where $m_W^{\rm ref}$ is the starting value, i.e. the measured value of m_W in a given publication, using generator predictions and PDF sets representing the state of the art at the time the measurement was prepared; $\delta m_W^{\rm QCD}$ represents the effect of using improved final state distributions for the same initial PDF set; and $\delta m_W^{\rm PDF}$ represents the extrapolation to a newer PDF set. The "−" signs reflect our convention to define the shifts δm_W from fits of templates produced with the reference QCD model and PDF set used by the experiments to pseudo-data with updated QCD or PDF predictions; fits of updated templates to unchanged data result in the opposite effect. It was checked, using relevant combinations of samples made from different generators and PDFs, that it was legitimate to estimate the corrections separately, i.e. that $\delta m_W^{\rm QCD+PDF} = \delta m_W^{\rm QCD} + \delta m_W^{\rm PDF}$.

For a proper evaluation of the PDF uncertainties and correlations, the latter need to be evaluated for all existing measurement channels or categories, and combined. This includes six measurements for CDF (with fits to the $p_{\rm T}^{\ell}$, $m_{\rm T}$ and $E_{\rm T}^{\rm miss}$ distributions in the $W \to e\nu$ and $\mu\nu$ channels); two measurements for D0 (fits to the $p_{\rm T}^{\ell}$ and $m_{\rm T}$ distributions in the $W \to e\nu$ channel), and 28 measurement categories for ATLAS (with fits to the $p_{\rm T}^{\ell}$ and $m_{\rm T}$ distributions in the $W \to e\nu$, and $W \to \mu\nu$ channels, with three and four pseudorapidity categories respectively, separately for W^+ and W^- events). Combinations are performed using the BLUE method [64], as was used in all published measurements. The procedure is validated by comparing the uncertainties obtained for the PDFs to their counterparts reported in the past publication. Partial combinations, reproducing published numbers for the individual CDF, D0 and ATLAS combinations, for the TeVatron combination, and for subsets of the ATLAS measurement categories, provide further validation. Finally, a complete combination can be performed.

This procedure is repeated for a representative ensemble of current PDF sets, to evaluate the model dependence of the PDF correlations. The combined values of m_W are then to be compared for various PDF sets, and a final prescription given to define the reference combined value.

5 Measurement emulation

In this section, the analysis procedures employed by ATLAS, CDF and D0 are summarized. This includes a description of the basic event selections and fitting ranges, and a simplified description of the detector resolutions. Simplified emulations of ATLAS, CDF, and D0 are set up to avoid using the full simulation chain of each collaboration which would be nearly impossible given the amount of needed computing resources. The corresponding implementation is shown to be adequate to evaluate the impact of modifications in the generator-level distributions on the determination of m_W.

The simplified simulations, or emulations, could be avoided in favour of distributions produced using the actual simulation of the experiments, or of migration and efficiency matrices, produced using this simulation, and describing the correlation between the generator-level and detector-level final state distributions m_{T}, p_{T}^{ℓ} and $E_{\mathrm{T}}^{\mathrm{miss}}$. Distributions would be costly to produce for a large set of QCD and PDF variations, and migration matrices are not available from the experiments at present. The implementation below is offered as an alternative. The accuracy is discussed below, as well as the associated systematic uncertainties.

In the following, $u_{\parallel}$ and $u_{\perp}$ are defined as the projections of the recoil u_{T} on the axes parallel and perpendicular to the W boson line of flight.

5.1 Event selections, fit ranges and measurement categories

Event selections and fitting ranges for the three measurements are summarized in Table 3. Selections and ranges are applied at detector level; a parametrisation of the CDF, D0 and ATLAS detector resolutions is described in the next sections.

CDF and D0 use very similar analysis configurations. The looser recoil cut and wider m_{T} fit range in ATLAS are a consequence of the worse recoil resolution. The multijet background is enhanced in ATLAS due to the worse recoil resolution and the higher collision energy; the tighter p_{T}^{ℓ} fit range mitigates this effect.

Experiment	Event selections	Fit ranges
CDF	$30 < p_{\mathrm{T}}^{\ell} < 55$ GeV, $\lvert\eta_{\ell}\rvert < 1$ $30 < E_{\mathrm{T}}^{\mathrm{miss}} < 55$ GeV, $60 < m_{\mathrm{T}} < 100$ GeV $u_{\mathrm{T}} < 15$ GeV	$32 < p_{\mathrm{T}}^{\ell} < 48$ GeV $32 < E_{\mathrm{T}}^{\mathrm{miss}} < 48$ GeV $65 < m_{\mathrm{T}} < 90$ GeV
D0	$p_{\mathrm{T}}^{\ell} > 25$ GeV, $\lvert\eta_{\ell}\rvert < 1.05$ $E_{\mathrm{T}}^{\mathrm{miss}} > 25$ GeV, $m_{\mathrm{T}} > 50$ GeV $u_{\mathrm{T}} < 15$ GeV	$32 < p_{\mathrm{T}}^{\ell} < 48$ GeV $65 < m_{\mathrm{T}} < 90$ GeV
ATLAS	$p_{\mathrm{T}}^{\ell} > 30$ GeV, $\lvert\eta_{\ell}\rvert < 2.4$ $E_{\mathrm{T}}^{\mathrm{miss}} > 30$ GeV, $m_{\mathrm{T}} > 60$ GeV $u_{\mathrm{T}} < 30$ GeV	$32 < p_{\mathrm{T}}^{\ell} < 45$ GeV $66 < m_{\mathrm{T}} < 99$ GeV

Table 3: Event selections and fit ranges for CDF, D0 and ATLAS.

CDF performs measurements in the $W \to e\nu$ and $W \to \mu\nu$ channels, using template fits to the p_{T}^{ℓ}, m_{T} and $E_{\mathrm{T}}^{\mathrm{miss}}$ distributions, *i.e* six measurements. D0 uses the p_{T}^{ℓ} and m_{T} distributions in the $W \to e\nu$ channel only.

These measurements are performed inclusively in pseudorapidity and summing over W^+ and W^- decays. ATLAS measures W^+ and W^- events separately, as in pp collisions the final state distributions are different for these processes. In addition, the analyzed pseudorapidity range is separated into three categories in the electron channel, and four categories in the muon channel, yielding a total of 28 measurements.

The emulation procedure starts from applying resolution and response corrections to leptons defined at the Born-level. The impact of choosing bare or dressed leptons is found to be negligible. Recoil resolutions are then applied to the W-boson transverse momentum, and the derived quantities ($E_{\mathrm{T}}^{\mathrm{miss}}$, m_{T}) are computed. Event selections and m_W fitting ranges are then applied as summarized in Table 3.

5.2 Parameterisation of the CDF experimental resolutions

The CDF detector response and resolution is modelled using a simulation based on a parameterization of the resolutions taken from the 2.1 fb^{-1} CDF measurement [18], which are expected to differ only slightly with respect to the current measurement [1].

The recoil response functions for CDF are parameterised in terms of the recoil magnitude and angular resolution as described in the published paper. Defining $p_{\mathrm{T}}^{\mathrm{ref}} = 15$ GeV, the recoil response $R(p_{\mathrm{T}}^W) \equiv -\langle u_{\parallel} \rangle / p_T^W$ and sampling term $\sigma_{u_{\mathrm{T}}}$ are given by:

$$R(p_{\mathrm{T}}^W) = 0.645 \times \log\Big(5.1 \times p_{\mathrm{T}}^W + 8.2\Big)/\log\Big(5.1 \times p_{\mathrm{T}}^{\mathrm{ref}} + 8.2\Big), \tag{4}$$

$$\sigma_{u_{\mathrm{T}}}(p_{\mathrm{T}}^W) = 0.82 \times \sqrt{p_{\mathrm{T}}^W}\ \mathrm{GeV}. \tag{5}$$

For $p_{\mathrm{T}}^W < p_{\mathrm{T}}^{\mathrm{ref}}$, the recoil angular resolution σ_{u_ϕ} is

$$\sigma_{u_\phi}(p_{\mathrm{T}}^W) = 0.306 + 0.021 \times (9.4 - p_{\mathrm{T}}^W)\ \mathrm{rad}; \tag{6}$$

while for $p_{\mathrm{T}}^W > p_{\mathrm{T}}^{\mathrm{ref}}$ it becomes

$$\sigma_{u_\phi}(p_{\mathrm{T}}^W) = 0.144 + 0.0048 \times (24.5 - p_{\mathrm{T}}^W)\ \mathrm{rad}. \tag{7}$$

The contribution of the underlying event to the measured recoil is represented by a randomly-oriented Gaussian distribution of width 5.2 GeV. Finally, 360 MeV is subtracted from the recoil along the direction of the decay lepton, to simulate the lepton removal procedure.

The electron resolution is modelled using a sampling term of $12.6\%/\sqrt{E_{\mathrm{T}}}$ and a 2% constant term to correct for the lack of final-state radiation in the generated samples.

Comparisons between the distributions obtained from the official CDF simulation [18] and the present emulation are shown in Figure 2. The simulated and emulated samples are reweighted to the reference p_{T}^W distribution for CDF shown in Fig. 1, and agree within 1% in the range of interest for the W mass extraction. The recoil and electron resolution functions described above are independently varied by ±5% to estimate the systematic uncertainties associated to this approximate simulation, and cover for differences between Refs. [18] and [1].

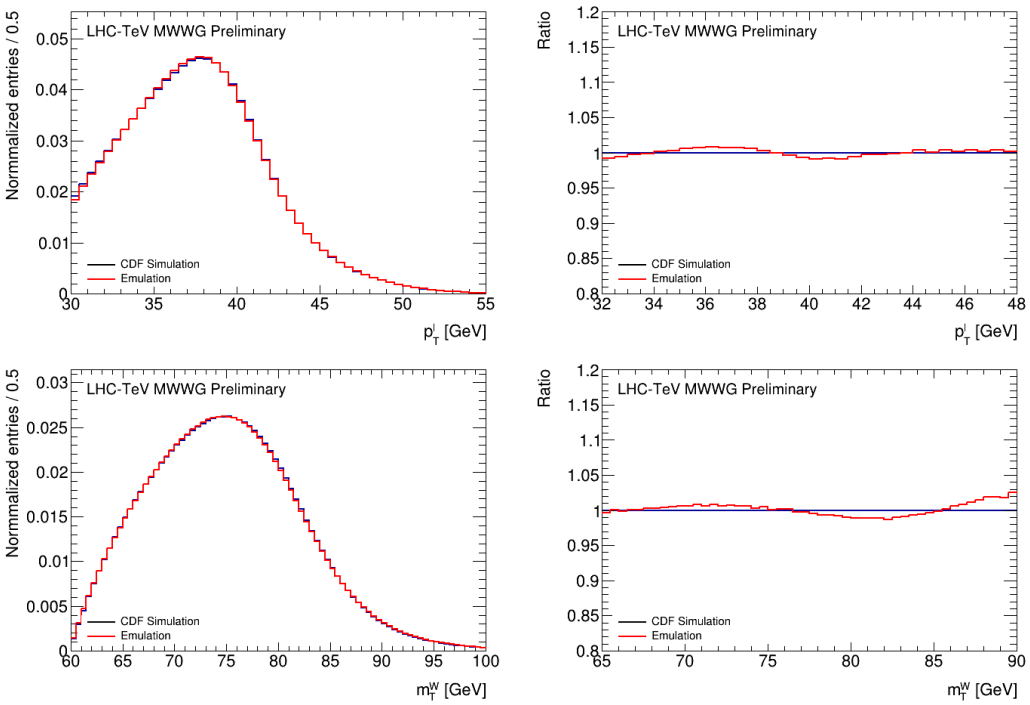

Figure 2: Comparison of the published [18] and simulated p_{T}^{ℓ} (top) and m_{T} (bottom) distributions for CDF using the emulation described in the text. Overlays are shown on the left; the ratio panels on the right are restricted to the corresponding fitting ranges, and include the resolution uncertainty variations described in the text.

5.3 Parameterisation of the D0 experimental resolutions

For D0, the three main characteristics of the event reconstruction, namely the electron energy measurement, the electron reconstruction and selection efficiency, and the recoil measurement were emulated separately. The emulation is based on the 4.3 fb^{-1} analysis. The response in the 1.1 fb^{-1} Run2a analysis is expected to be largely the same, but for a better recoil resolution due to the lower pile-up conditions accounted for by inflating its systematic uncertainty for this dataset.

5.3.1 Electron resolution

The electron resolution is simulated by a Gaussian smearing with standard deviation σ_{EM} following Ref. [3] as

$$\frac{\sigma_{\mathrm{EM}}}{E_0} = \sqrt{C_{\mathrm{EM}}^2 + \frac{S_{\mathrm{EM}}^2}{E_0} + \frac{N_{\mathrm{EM}}^2}{E_0^2}}, \tag{8}$$

where E_0, C_{EM}, S_{EM}, and N_{EM} represent the uncorrected electron energy, the constant term, the sampling term and the noise term, respectively. We take $N_{\mathrm{EM}} = 0$, $C_{\mathrm{EM}} = 0.01997$ as reported in Ref. [3], though the D0 analysis did include an explicit model of the underlying event contributions. The sampling term follows a more complex behavior:

$$S_{\mathrm{EM}} = S_0 \exp\left[S_1\left(\frac{1}{\sin\theta} - 1\right)\right] + \frac{S_2\eta + S_3}{\sqrt{E_0}}, \tag{9}$$

where $S_0 = 0.153$ GeV$^{1/2}$, $S_1 = 1.543$, $S_2 = -0.025$, and $S_3 = 0.172$ GeV. The overall resolution term obtained in this way, $\sigma_{\rm EM}$, is further increased by 2% to optimize the agreement with the reference distributions.

The electron energy response is parameterised as follows :

$$E = \alpha(E_0 - \bar{E}_0) + \beta + \bar{E}_0 \tag{10}$$

where E is the calibrated electron energy, $\bar{E}_0 = 43$ GeV is a reference value for the electron energy in Z-boson events; α and β are luminosity-dependent energy scale and offset corrections, respectively. We take $\alpha = 1.0164$ and $\beta = 0.188$ GeV, the values determined in Ref. [3] for an instantaneous luminosity, L, between $(2 < L < 4) \times 36 \times 10^{30}$cm^{-2}s^{-1}, which represents the largest fraction of the data[4].

5.3.2 Electron efficiency

The reconstruction and identification efficiency is modeled by the function

$$\varepsilon(p_{\rm T}^{\ell}) \quad = \quad 0.95\left(1 - e^{-0.074 p_{\rm T}^{\ell}}\right), \tag{11}$$

which fits the data points from Fig. 25(b) of Ref. [3].

5.3.3 Recoil smearing

The approach relies on randomly picking a u_T value for a given true p_T^W following a migration matrix with 1 GeV bins, and different azimuthal intervals. An example of a migration matrix is shown in Figure 3. These migrations are provided by the D0 Collaboration, and follow Ref. [65].

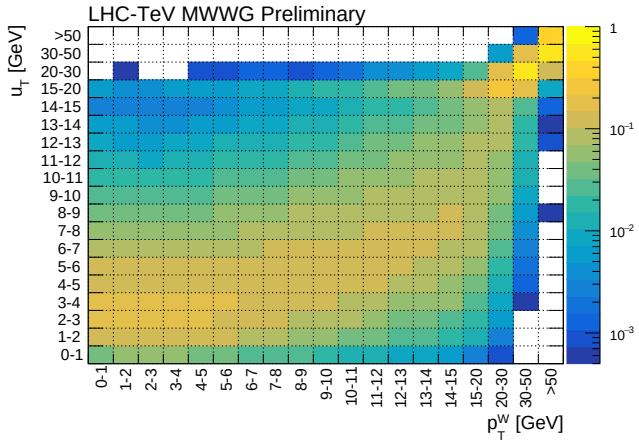

Figure 3: Migration matrix of the reconstructed W boson transverse momentum, u_T, as a function of the truth W boson, p_T^W in D0 experiment.

[4] It was tested that implementing the instantaneous luminosity dependence of the response parameters gives results in agreement to the 1% level to this "average" response

Approximately following Ref. [3], 150 MeV are subtracted from the component of the recoil parallel to the decay lepton, to account for electron cone effects. As in the case of CDF, relative uncertainties of 5% are assigned to the recoil and electron resolution functions described above, to estimate the systematic uncertainties associated to this approximate simulation.

5.3.4 Validation of the D0 emulation

Figure 4 shows comparisons between p_{T}^{ℓ} and m_{T} distributions from D0 PMCS (Parameterized Monte Carlo Simulation) used in the D0 publication and the outcome of the proposed emulation of the D0 response. The simulated and emulated samples are reweighted to the reference p_{T}^{W} distribution for D0 (cf. Fig. 1), and agree within 2% in the range of interest for the W mass extraction.

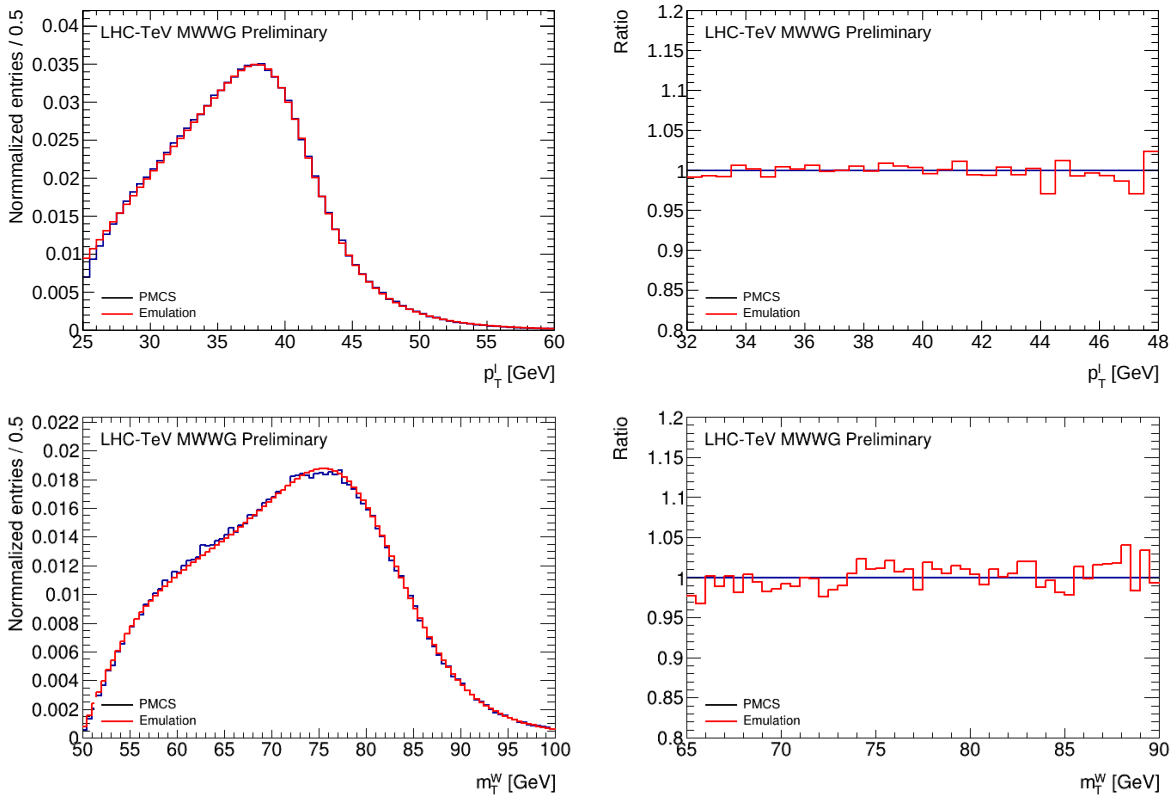

Figure 4: Comparison of the published and emulated p_{T}^{ℓ} (top) and m_{T} (bottom) distributions, for D0. Overlays are shown on the left; the ratio panels on the right are restricted to the corresponding fitting ranges, and include the resolution uncertainty variations described in the text.

Figure 5 illustrates the relative effect of given physics variations on the final-state distributions, using either PMCS or the present emulation. As a validation, the shifts in m_W obtained for the various eigenvectors of the CTEQ6.6 and CT10 PDFs for the emulation and the official D0 simulation PMCS have been compared, giving agreement to within 0.8 MeV.

In a further test, the effect of a correction of the angular coefficient A_0, corresponding to the difference between ResBos1 and ResBos2 for this quantity and discussed in Section 6.2, is compared for the present emulation and the results of the PMCS. The emulation uses $2.5{\times}10^8$ events, while the PMCS samples

is smaller with about 5.5×10^5 events. The corresponding shifts in m_W are compared in Table 4. Since these shifts are calculated using statistically correlated samples, the reported statistical uncertainties are estimated using the bootstrap method [66]. Agreement is observed within the statistical uncertainty of the test. This leads to an estimate of the uncertainty due to the differences between emulation and detailed simulation of about 1 ± 2 MeV. Variations of the electron and recoil resolutions affect the estimates by about 0.1 MeV and less than 2 MeV respectively.

Given the results of the different validations tests, we retain the value of 2 MeV as a conservative estimate of the emulation systematic uncertainty for D0.

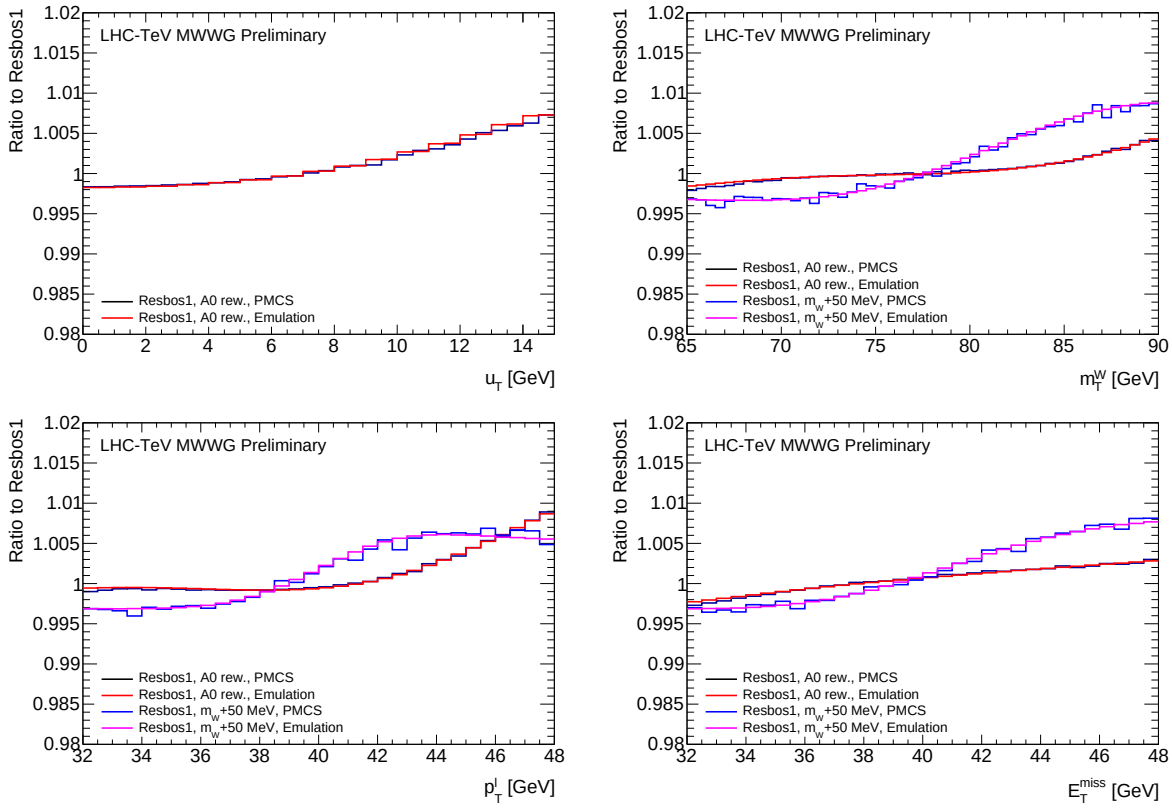

Figure 5: Ratio between the u_{T} (top left), m_{T} (top right), p_{T}^{ℓ} (bottom left) and $E_{\mathrm{T}}^{\mathrm{miss}}$ (bottom right) distributions obtained with and without the A_0 correction described in the text, for the D0 emulation and official simulation. For the fit distributions, the ratio is compared to the effect of a +50 MeV variation in m_W.

5.4 Parameterisation of the ATLAS experimental resolutions

For ATLAS, the recoil response is extracted from profiles of R, $\sigma_{u_{\parallel}}$ and $\sigma_{u_{\perp}}$ as a function of the W-boson transverse momentum, obtained from the simulation and corrected for calibration discrepancies. The recoil resolution is about 12–16 GeV, mostly depending on the amount of pile-up. The electron and muon resolutions are parameterised based on measured performance [67, 68].

Results are illustrated in Figure 6. The resolution is accurately modeled, and residual differences can be absorbed by lepton energy scale adjustments. These effects are found to not influence the emulation results significantly.

	δm_W [MeV]			
	D0 PMCS A_0 correction	This emulation A_0 correction	This emulation $\Delta\sigma_E/\sigma_E = \pm 5\%$	This emulation $\Delta\sigma_{\mathrm{uT}}/\sigma_{\mathrm{uT}} = \pm 5\%$
m_{T}	13.6 ± 1.9	12.6 ± 0.1	±0.1	±1.0
p_{T}^{ℓ}	16.3 ± 2.0	16.0 ± 0.1	±0.1	±1.0
$E_{\mathrm{T}}^{\mathrm{miss}}$	21.0 ± 2.2	19.5 ± 0.1	±0.1	±2.2

Table 4: Shifts in m_W under a change in the A_0 angular coefficient from its Resbos1 to the Resbos2 value. The shifts are expressed in MeV and corresponding to different physics variations, for PMCS and the present emulation. Systematic uncertainties corresponding to a 5% scaling of the electron and recoil resolution parameterisations are given as well.

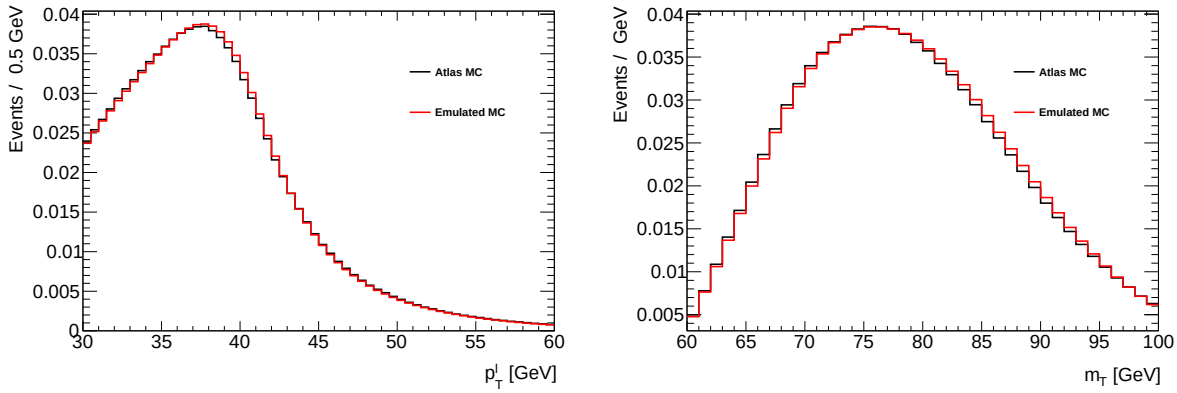

Figure 6: Comparison of the published and simulated p_{T}^{ℓ} (left) and m_{T} (right) distributions for ATLAS.

The precision of the emulated PDF-induced shifts in the fitted value of m_W is studied using the ATLAS measurement. With 28 measurement categories and 25 CT10nnlo PDF eigensets, a high-statistics comparison between the emulation and the full measurement procedure can be performed.

This comparison is performed in Figure 7, which illustrates the correlation between the published and emulated shifts for CT10nnlo. The shifts are defined as in Section 4: $\delta m_W^i = m_W^i - m_W^{\mathrm{ref}}$, where the reference set is the CT10nnlo central set, and the variations i are the uncertainty sets.

Analyzing all (25 symmetrized shifts for each of the 28 measurement categories), a spread of 1.5 MeV is found between the published and emulated shifts. Variations of the smearing procedures affect these results by less than 0.5 MeV; the residuals thus dominantly reflect different levels of approximation in the Powheg-based reweighting procedure used here, and the kinematic reweighting to NNLO-accurate distributions implemented in Ref. [4].

5.5 Recoil resolution comparisons

The ATLAS and CDF experiments are compared in terms of the recoil response function R, and recoil resolution functions $\sigma_{u_\parallel}$ and $\sigma_{u_\perp}$. R represents the ratio between the reconstructed and true transverse momentum of the W boson; the resolution of $u_\parallel$, $\sigma_{u_\parallel}$, is expected to be slightly larger than $\sigma_{u_\perp}$ due to the presence of hard radiation recoiling against the W boson. Results are illustrated in Figure 8. The D0 recoil

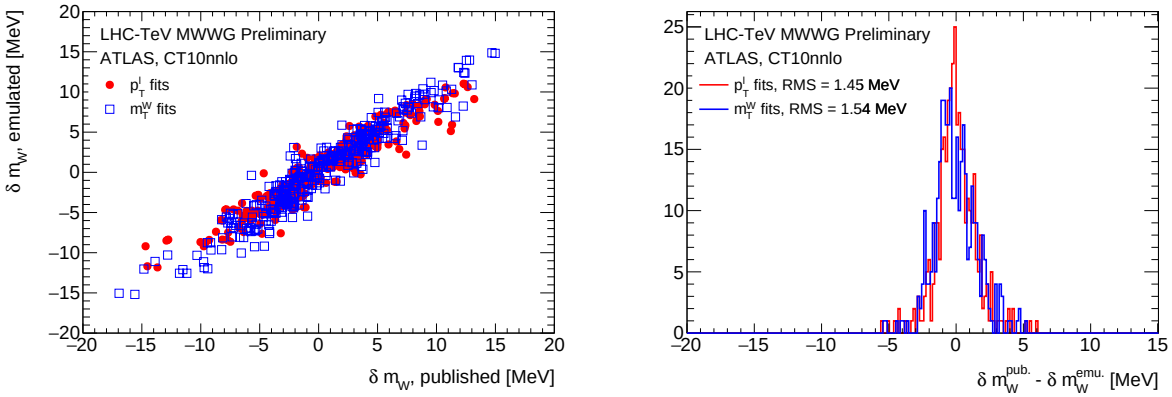

Figure 7: Left : correlation between the published and emulated CT10nnlo PDF shifts, in MeV, for the ATLAS measurement. Right : distribution of the differences between published and emulated shifts.

response and resolution are close to that of CDF. The CDF and D0 experiments both achieve a typical resolution of 4–5 GeV in the p_{T}^W range relevant for the measurement, while the higher centre-of-mass energy and pile-up in ATLAS yield a resolution of about 13 GeV.

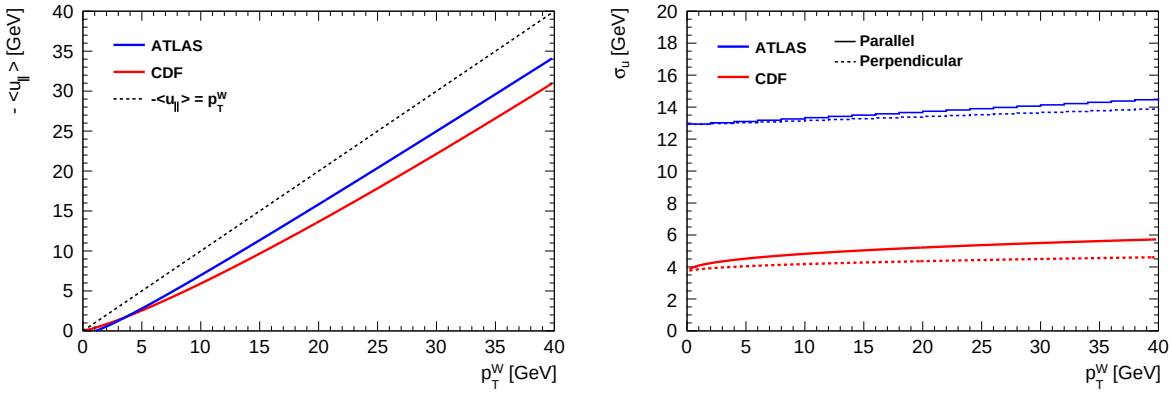

Figure 8: Comparison of the parameterised recoil response (left) and resolution (right) for ATLAS and CDF.

6 QCD modelling aspects

Differences in the QCD modelling between the different generators may motivate a correction of past measurements to account for improved theory predictions.

In this section we investigate in particular differences in the description of the invariant dilepton mass and boson rapidity distributions, and in the modelling of spin correlations in the boson decay.

6.1 Invariant mass and rapidity distribution in Resbos1

The full lepton phase-space W-boson invariant mass distributions are shown in Figure 9 for the CDF Resbos1 sample, Resbos2, and Powheg, where all predictions use the CTEQ6M PDF. The CDF sample

includes an invariant mass requirement of $m = 150$ GeV, and shows a small difference with respect to the other distributions for $m < 70$ GeV. Figure 10 show the same comparison for D0, with CTEQ6.6. There is no mass cut; a similar but smaller distortion than for CDF appears for $m < 50$ GeV in the D0 Resbos1 sample. These effects are likely related to artefacts in the Resbos pre-integration grids. Common to both comparisons is a small, long-range slope visible between Resbos1 and Resbos2 and Powheg.

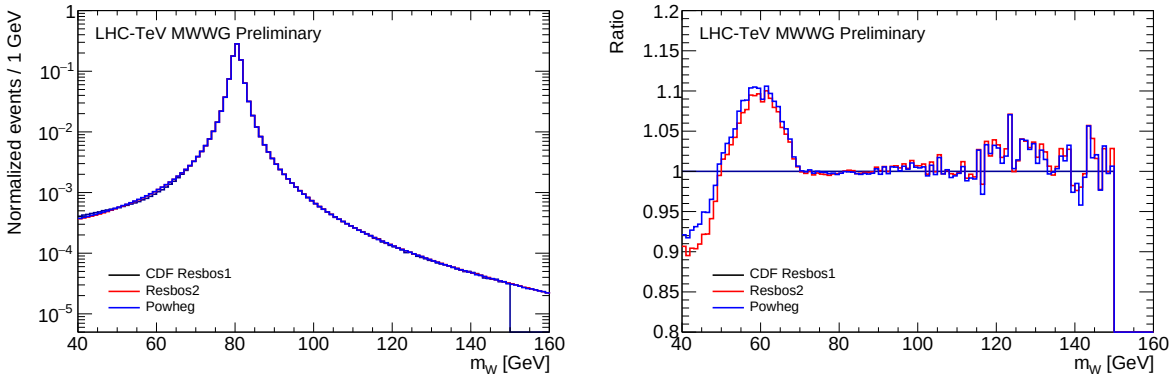

Figure 9: Left: Comparison between the invariant mass distributions in the CDF Resbos1 sample, Resbos2, and Powheg. All histograms use generated mass and width values of $m_W = 80.450$ GeV and $\Gamma_W = 2.120$ GeV. Right: Ratios with respect to the CDF Resbos1 sample.

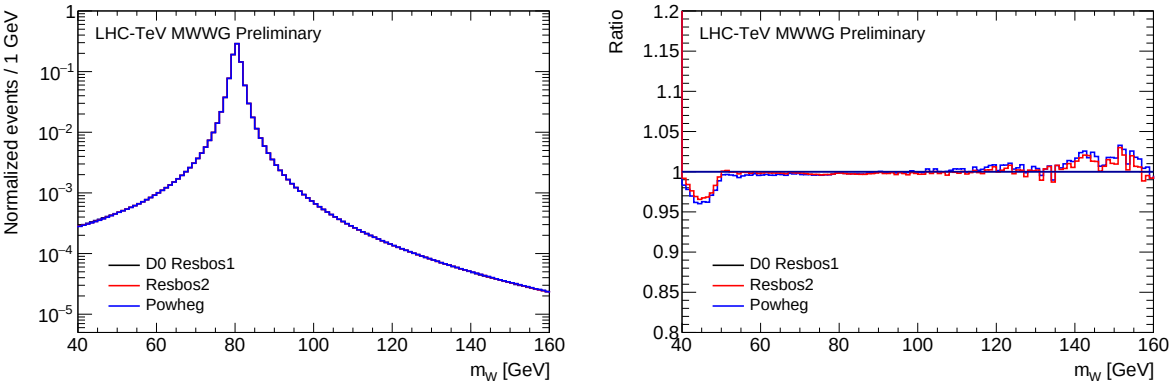

Figure 10: Left: Comparison between the invariant mass distributions in the D0 Resbos1 sample, Resbos2, and Powheg. All histograms use generated mass and width values of $m_W = 80.378$ GeV and $\Gamma_W = 2.046$ GeV. Right: Ratios with respect to the D0 Resbos1 sample.

The W-boson rapidity distributions are compared in the full lepton phase-space in Figure 11. CDF Resbos1 differs from Resbos2 for the CTEQ6M rapidity distribution by up to 2% near $y_W \sim 2.3$; these differences are assigned to the different Resbos versions used for both distributions. The D0 Resbos1 prediction is close to Resbos2 for CTEQ6.6, and differs from CTEQ6M by several percent, as can be expected from the different PDF sets used. The large differences observed between CDF Resbos1 and the other predictions for $|y_W| > 2.5$ reflect the differences in the invariant mass distributions discussed above.

The impacts of these differences are evaluated using the measurement emulation procedure outlined in Section 5. Templates of the p_{T}^{ℓ}, $E_{\mathrm{T}}^{\mathrm{miss}}$ and m_{T} distributions for different values of m_W are generated using the legacy CDF and D0 samples; one-dimensional reweightings of either the invariant mass or the rapidity

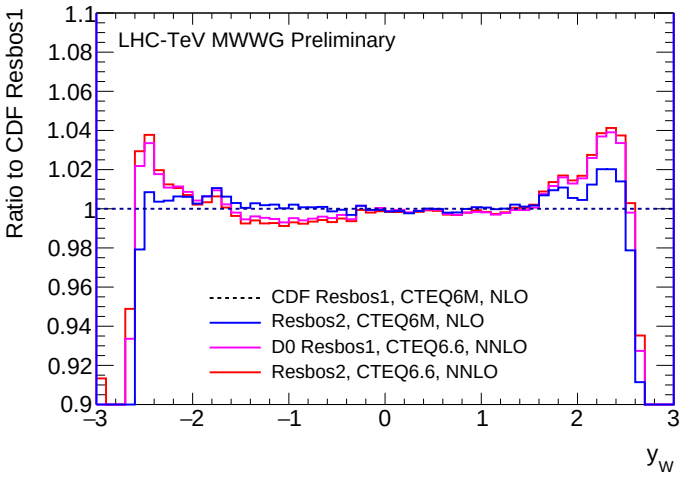

Figure 11: Ratio, with respect to the CDF Resbos1 sample (CTEQ6M), of the W^+-boson rapidity distributions in Resbos2 (CTEQ6M), the D0 Resbos1 sample (CTEQ6.6), and Resbos2 (CTEQ6.6). The invariant mass threshold in the CDF Resbos1 sample affects the region of large $|y|$.

distribution, according to Figures 9-11, define pseudo-data. The resulting shifts in m_W are reported in Table 5. The effect of the rapidity distortions are found to be negligible for both experiments. The same holds for the small effects observed in the D0 invariant mass distribution. For CDF, an effect of (2.1, 1.4, 2.7) MeV is found for the (p_{T}^{ℓ}, m_{T}, p_{T}^{ν}) fits, respectively, mostly due to the invariant mass cut.

6.2 Treatment of spin correlations in W-boson decays

The p_{T}^{ℓ} and m_{T} distributions are sensitive to the polar angle distribution of the decay leptons. Equation 1 shows that the A_0 and A_4 terms should dominate, since only these terms survive an integration over the lepton azimuth. A_0 primarily reflects the relative fractions of the $qq \to W$, $qg \to Wq$ and higher-order sub-processes, and shows a strong p_{T}^{W} dependence while being nearly independent of rapidity. A_4 is a forward-backward asymmetry, and primarily reflects the directions of the incoming quark and anti-quark in the dominant $qq \to W$ process. It strongly depends on rapidity and on the PDF set assumed for the calculation, and slowly decreases with p_{T}^{W}.

6.2.1 Angular coefficients in the CDF and D0 measurements

We find that the behaviour of the spin correlations in the ResBos C and ResBos CP codes differs from that of fixed-order calculations (e.g. MCFM [69], DYNNLO [61], FEWZ [70]) or modern Monte Carlo generators such as Herwig [71] or MiNNLO [46], which agree among each other. In addition all of these predictions are found in agreement with measurements of the angular coefficients at the LHC [62]. The updated version of Resbos, ResBos2, was brought in agreement with the aforementioned calculations, and with the data.

Each angular coefficient A_i is the ratio of the corresponding helicity cross section to the unpolarized cross section:

$$A_i = \frac{\sigma_i}{\sigma_{\mathrm{unpol}}}, \tag{12}$$

where the A_i are understood to be functions of the vector boson kinematics, i.e. p_{T}, y, and m, and where σ_i stands for the differential cross section $\mathrm{d}^3\sigma/\mathrm{d}p_{\mathrm{T}}\mathrm{d}y\mathrm{d}m$, for the polarization state i. In ResBos1, only the unpolarized cross section, $\sigma_{\mathrm{unpol}} \propto (1+\cos^2\theta)$, and the forward backward asymmetry, $\sigma_4 \propto A_4 \cos\theta$, are changed by the resummation, whereas σ_{0-3} are left at fixed order. This implies, for the angular coefficients:

$$A_{0-3}^{\mathrm{ResBos1}} = \frac{\sigma_{0-3}^{\mathrm{F.O.}}}{\sigma_{\mathrm{unpol}}^{\mathrm{Res.}}}, \qquad A_4^{\mathrm{ResBos1}} = \frac{\sigma_4^{\mathrm{Res.}}}{\sigma_{\mathrm{unpol}}^{\mathrm{Res.}}}. \tag{13}$$

While the unpolarized and A_4 contributions to the cross section display natural p_{T}^W and p_{T}^Z distributions, the polarized contributions diverge at low transverse momentum. In ResBos2, all helicity cross sections are resummed, resulting in:

$$A_{0-4}^{\mathrm{ResBos2}} = \frac{\sigma_{0-4}^{\mathrm{Res.}}}{\sigma_{\mathrm{unpol}}^{\mathrm{Res.}}}, \tag{14}$$

considering universal resummation corrections. The latter implies the following relations, for $A_0 - A_3$:

$$\frac{A_{0-3}^{\mathrm{ResBos2}}}{A_{0-3}^{\mathrm{ResBos1}}} = \frac{\sigma_{0-3}^{\mathrm{Res.}}}{\sigma_{0-3}^{\mathrm{F.O.}}} = \frac{\sigma_{\mathrm{unpol.}}^{\mathrm{Res.}}}{\sigma_{\mathrm{unpol.}}^{\mathrm{F.O.}}}, \tag{15}$$

and

$$A_{0-3}^{\mathrm{ResBos2}} \equiv \frac{\sigma_{0-3}^{\mathrm{Res.}}}{\sigma_{\mathrm{unpol.}}^{\mathrm{Res.}}} = \frac{\sigma_{0-3}^{\mathrm{F.O.}}}{\sigma_{\mathrm{unpol.}}^{\mathrm{F.O..}}}. \tag{16}$$

In other words, the ratio between the angular coefficients in ResBos2 and ResBos1 should match the ratio between the resummed and fixed-order unpolarized cross sections; in particular, the p_{T} dependence of $A_i^{\mathrm{ResBos2}}/A_i^{\mathrm{ResBos1}}$ should match the ratio of the resummed and fixed-order p_{T} distributions. According to the second relation, the consistent resummation of all helicitity cross sections preserves the fixed-order behaviour of the angular distributions.

Figure 12 qualitatively illustrates the effects expected from the above equations. The ratios between the ResBos2 and ResBos1 predictions for A_{0-3} are observed to be close, and match the ratio between resummed and fixed-order p_{T} distributions. The latter is calculated using ResBos1 at NLO+NLL, and MCFM at NLO.

Figures 13 and 14 compare A_0 to A_4 in W-boson events at 1.96 TeV, for ResBos1, DYNNLO, ResBos2 and MiNNLO. The DYNNLO, ResBos2 and MiNNLO predictions are given at $O(\alpha_{\mathrm{s}})$, $O(\alpha_{\mathrm{s}})$ and $O(\alpha_{\mathrm{s}}^2)$ respectively. As mentioned above, good agreement is observed between these predictions, while ResBos1 deviates from the others. The fixed-order and MiNNLO generators are consistent with measurements of Z-boson production, as shown in Ref. [62]. The p_{T}^W dependence of all coefficients is found to be softer in ResBos1, both for the versions used by CDF, and by D0. In addition, while A_0 is expected to converge to 0 at p_{T}^W =0, the Resbos1 predictions reach $A_0(p_{\mathrm{T}}^W = 0) \sim 0.003$. These features motivate a correction to the physical behaviour of the ResBos2 calculation, which is also theoretically preferred and in agreement with measurements.

The difference in the p_{T}^W dependence of the A_i appears to be the most significant between the calculations, while the rapidity dependence agrees well between generators.

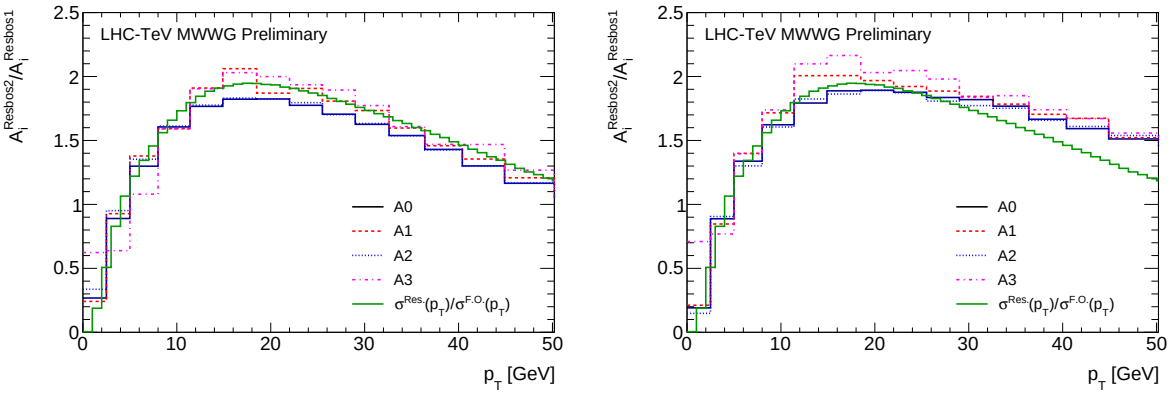

Figure 12: Ratio between the ResBos2 and ResBos1 predictions from CDF (left) and D0 (right) for $A_0 - A_3$, as a function of p_{T}^W. The ratio between the p_{T}^W distributions at NLO+NLL from ResBos1, and at NLO from MCFM is overlaid for comparison. .

6.2.2 Angular coefficients in the ATLAS measurement

Figure 15 compares A_0 and A_2 in W^+ and W^- events at 7 TeV, for Powheg and DYNNLO, at $O(\alpha_s)$, using the CT10nnlo PDF. The two predictions are in good agreement in the high-p_{T}^W region, while Powheg exhibits a negative value for A_0 at low p_{T}^W, $A_0(p_{\mathrm{T}}^W = 0) \sim -0.05$. This is a known feature, first observed in e.g. Refs [62, 72]. In the measurement, Powheg was corrected to DYNNLO at $O(\alpha_s^2)$, and the corresponding uncertainties were assigned. An update is in this case not justified.

6.3 Impact on the final state distributions

Following Eq. 1, the effect of modifications to the different angular coefficients can be evaluated by applying an event weight as follows:

$$w_{A_i \to A_i'}(\cos\theta, \phi; p_{\mathrm{T}}^W, y_W) = \frac{(1+\cos^2\theta) + \sum_i A_i'(p_{\mathrm{T}}^W, y_W) f_i(\theta;\phi)}{(1+\cos^2\theta) + \sum_i A_i(p_{\mathrm{T}}^W, y_W) f_i(\theta;\phi)}, \tag{17}$$

where the f_i are the functions of θ and ϕ shown in Eq. 1, A_i are the angular coefficients of the initial prediction and A_i' those of the target prediction. The A_i are pre-calculated for all generators at hand, in intervals of boson p_{T}, y and m, using

$$\begin{aligned}
A_0 &= \frac{2}{3} + \frac{10}{3} < 1 - 3\cos^2\theta > \\
A_1 &= 5 < \sin 2\theta \cos\phi > \\
A_2 &= 10 < \sin^2\theta \cos 2\phi > \\
A_3 &= 4 < \sin\theta \cos\phi > \\
A_4 &= 4 < \cos\theta > \\
A_5 &= 5 < \sin^2\theta \sin 2\phi > \\
A_6 &= 5 < \sin 2\theta \sin\phi > \\
A_7 &= 4 < \sin\theta \sin\phi >
\end{aligned} \tag{18}$$

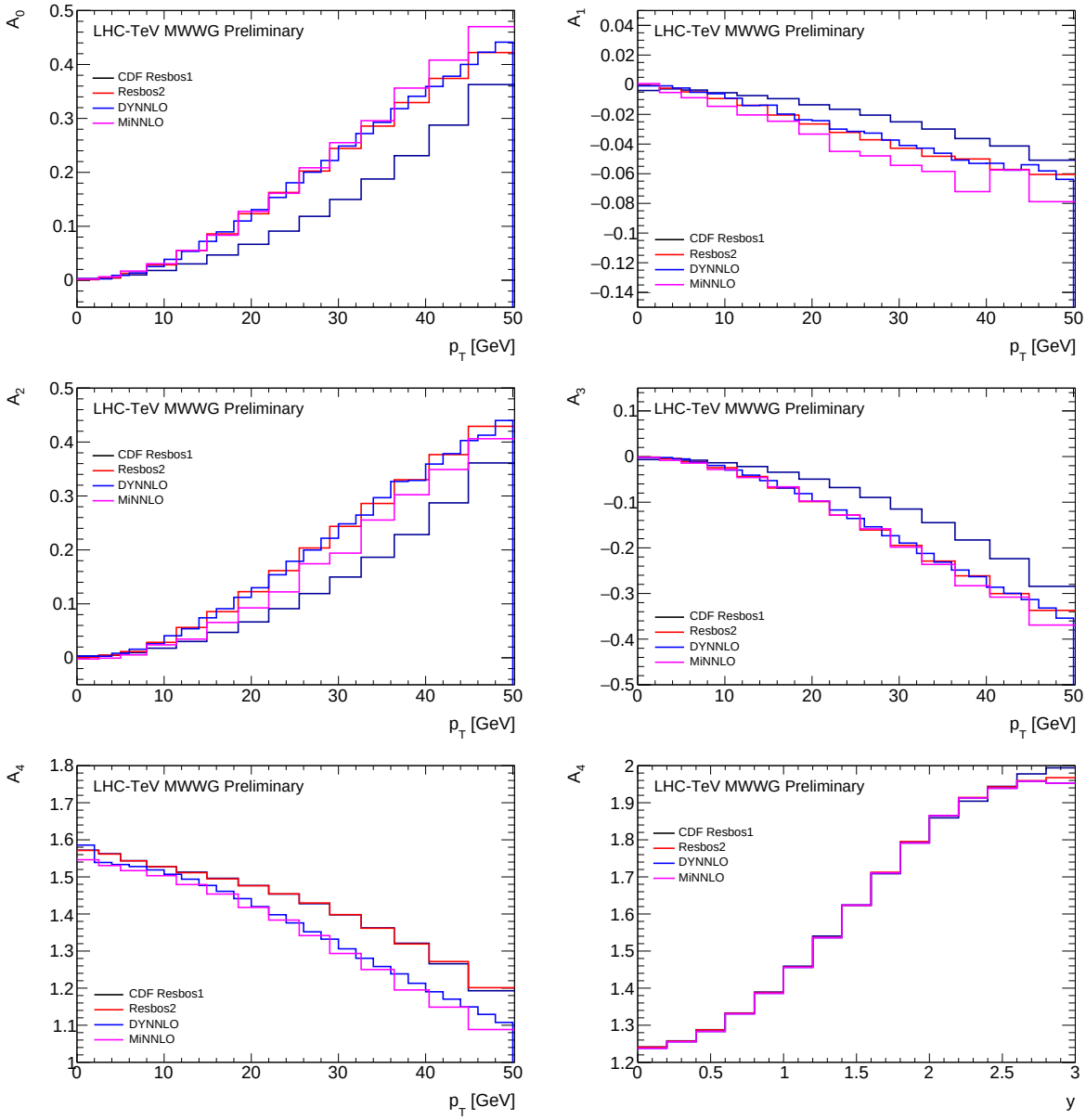

Figure 13: $A_0 - A_4$ as a function of p_{T}^W, and A_4 as a function of y_W, extracted from the CDF legacy Resbos sample and as predicted by DYNNLO, MiNNLO and ResBos2, with the CTEQ6M PDF set, in $p\bar{p}$ collisions at 1.96 TeV.

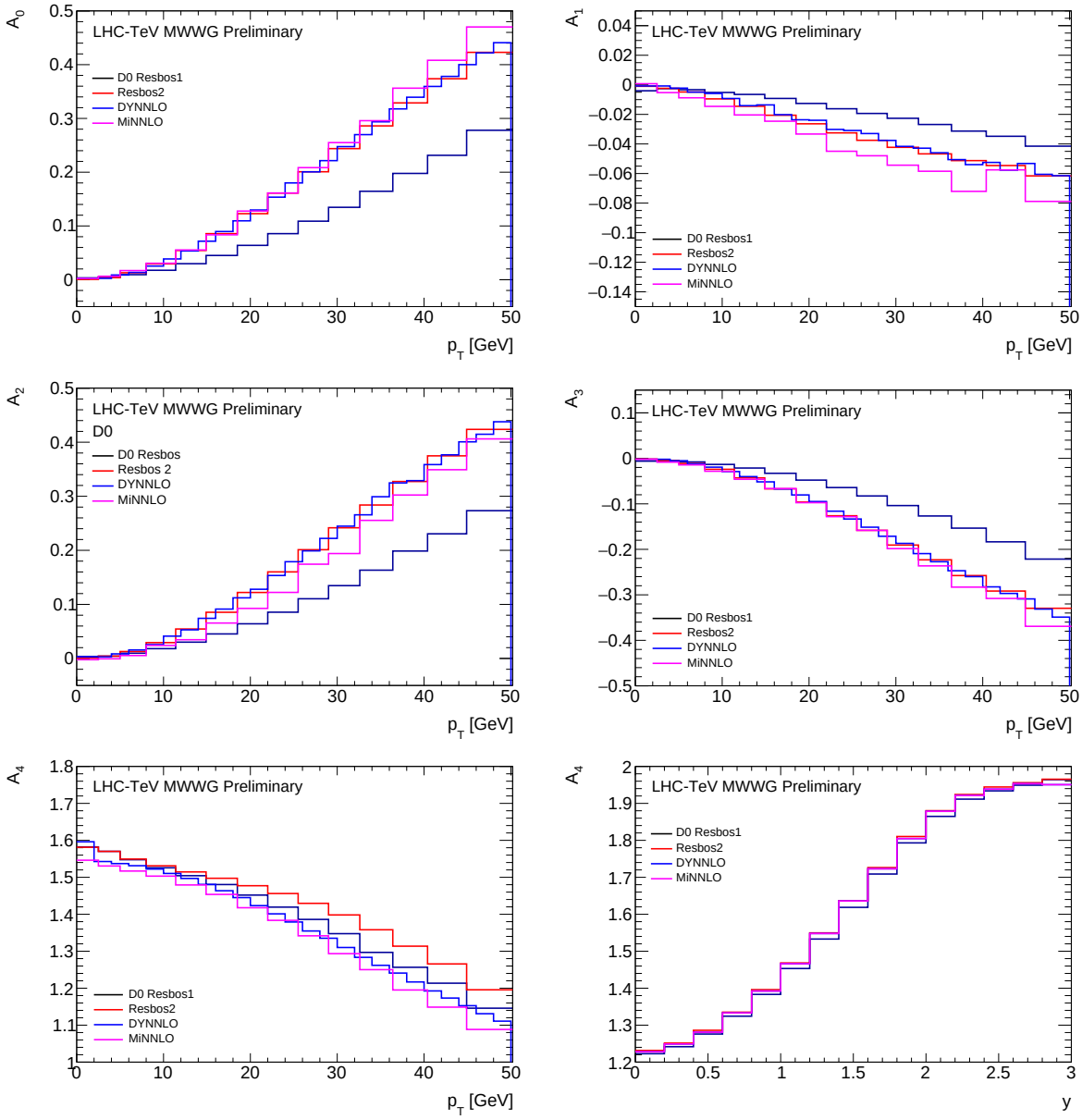

Figure 14: $A_0 - A_4$ as a function of p_{T}^W, and A_4 as a function of y_W, extracted from the D0 legacy Resbos grids and as predicted by DYNNLO, MiNNLO and ResBos2, with the CTEQ6.6 PDF set, in $p\bar{p}$ collisions at 1.96 TeV.

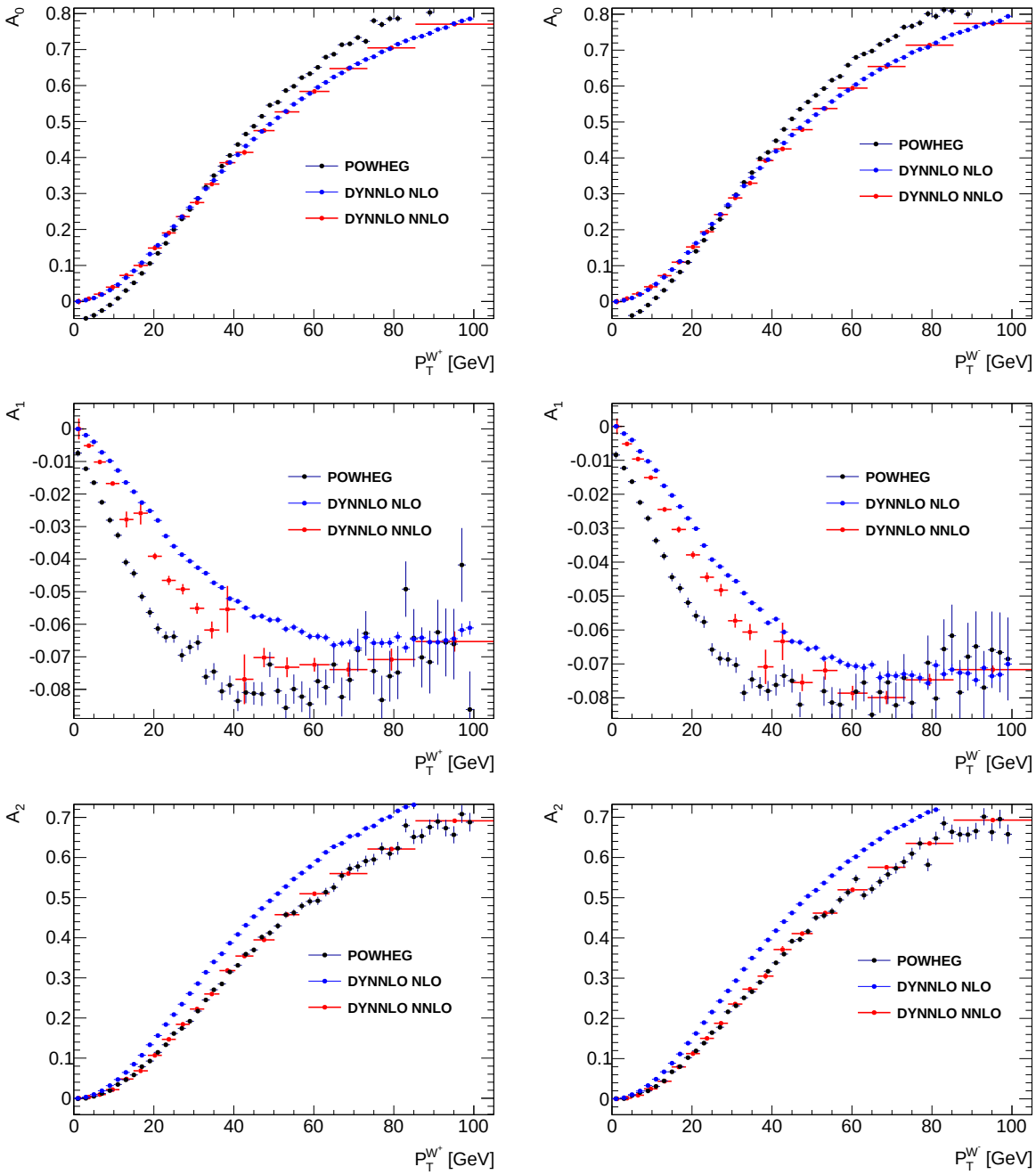

Figure 15: $A_0 - A_2$ as a function of p_{T}^W as predicted by POWHEG, DYNNLO at $O(\alpha_{\mathrm{s}})$ and DYNNLO at $O(\alpha_{\mathrm{s}}^2)$, for W^+ and W^- production in pp collisions at 7 TeV.

where all averages are calculated in the full solid angle of the decay leptons. This procedure then allows decomposing the contributions of the lepton angular distributions to the differences observed between two Monte Carlo predictions, globally as well separately for each coefficient.

The effects on the final state distributions are illustrated in Figures 16 and 19 for CDF, and 17 and 18 for D0. The CDF and D0 measurements are based on ResBos1, which prompts the present discussion. The ATLAS measurement, based on Powheg, already incorporates a correction to the fixed-order prediction of DYNNLO, at $O(\alpha_s^2)$, and assigns corresponding systematic uncertainties [4]. The recent measurement by LHCb also addresses these issues quantitatively [5].

Figures 16 and 17 illustrate the reweighting of the ResBos1 final state distributions to ResBos2. The left columns show the impact of each coefficient, as well as the impact of the combined coefficients for the generated p_T^W, the reconstructed p_T^W, m_T, and p_T^ℓ distributions. As can be expected, modifying the lepton decay angle distributions affects the final state distributions after analysis cuts. The selected, generator-level $p_{\rm T}^W$ distribution changes with an amplitude of about 2%, of which about 1% remains at detector level. The $m_{\rm T}$ distributions change by about 0.5% at high values, and the $p_{\rm T}^\ell$ distribution modulates by about 1.5%, with partly compensating slopes at low and high values.

A similar bias affects Z production, for which the predicted $p_{\rm T}$ distribution is fitted to the data, adjusting the non-perturbative resummation parameters. Assuming the effects of spin correlation biases to be similar in W and Z production, their effect on the fiducial $p_{\rm T}^W$ distribution can be expected to be in part absorbed by the resummation fit in Z events. While this implies the interpretation of the fitted values of $g_{1,2}$ is subject to caution, one can approximate the effect of this fit by imposing that the final-state $p_{\rm T}^W$ distribution should not change, multiplying the spin correlation weight by an additional event weight correcting the selected $p_{\rm T}^W$ distribution back to its initial shape:

$$w^{\rm corr}_{A_i\to A'_i}(p_{\rm T}^W) \equiv \left(\frac{1}{\sigma_W^{\rm sel.}}\frac{d\sigma_W^{\rm sel.}}{dp_{\rm T}}\right)_{A_i} \Bigg/ \left(\frac{1}{\sigma_W^{\rm sel.}}\frac{d\sigma_W^{\rm sel.}}{dp_{\rm T}}\right)_{A'_i}, \tag{19}$$

$$w^{tot}_{A_i}(\cos\theta,\phi;p_{\rm T}^W,y_W) = w_{A_i\to A'_i}(\cos\theta,\phi;p_{\rm T}^W,y_W)\times w^{\rm corr}_{A_i\to A'_i}(p_{\rm T}^W). \tag{20}$$

The results of this procedure are illustrated in the right columns of Figs. 16 and 17. The selected $p_{\rm T}^W$ and $u_{\rm T}$ distributions are now unchanged by construction, and the impact on the $m_{\rm T}$ and $p_{\rm T}^\ell$ distributions is correspondingly reduced. A similar approach is used for PDF extrapolations in Section 7.1.

This approach assumes that any modifications to the $p_{\rm T}^W$ distribution due to changes in PDFs and angular coefficients are corrected by the experimental fit of the parameters describing the $p_{\rm T}^Z$ and $p_{\rm T}^W$ distributions to $p_{\rm T}^Z$ data. A more accurate estimate requires an evaluation of the correlations of these physics effects on the W and Z distributions, and should account for the experimental uncertainty in the $u_{\rm T}$ distribution. This is beyond the scope of the current analysis.

The expected impact on the D0 measurement is reported in Figure 18 and Table 5. The initial distributions, the reweighted distributions, and the ResBos2 predictions are compared after including the detector emulation. The effects in the rapidity and invariant mass distributions, discussed in Section 6.1, do not have a significant impact. The following lines give the impact of correcting A_0 to A_4 separately, and simultaneously; the latter matches the sum of the individual corrections, as expected. The total effect of the invariant mass, rapidity, and A_i corrections are given in the "Total" line. The "ResBos2" line shows the result of direct fits of ResBos1 to ResBos2, which match the sum of the successive corrections to ResBos1, indicating that the differences are understood quantitatively. The A_i reweighting qualitatively

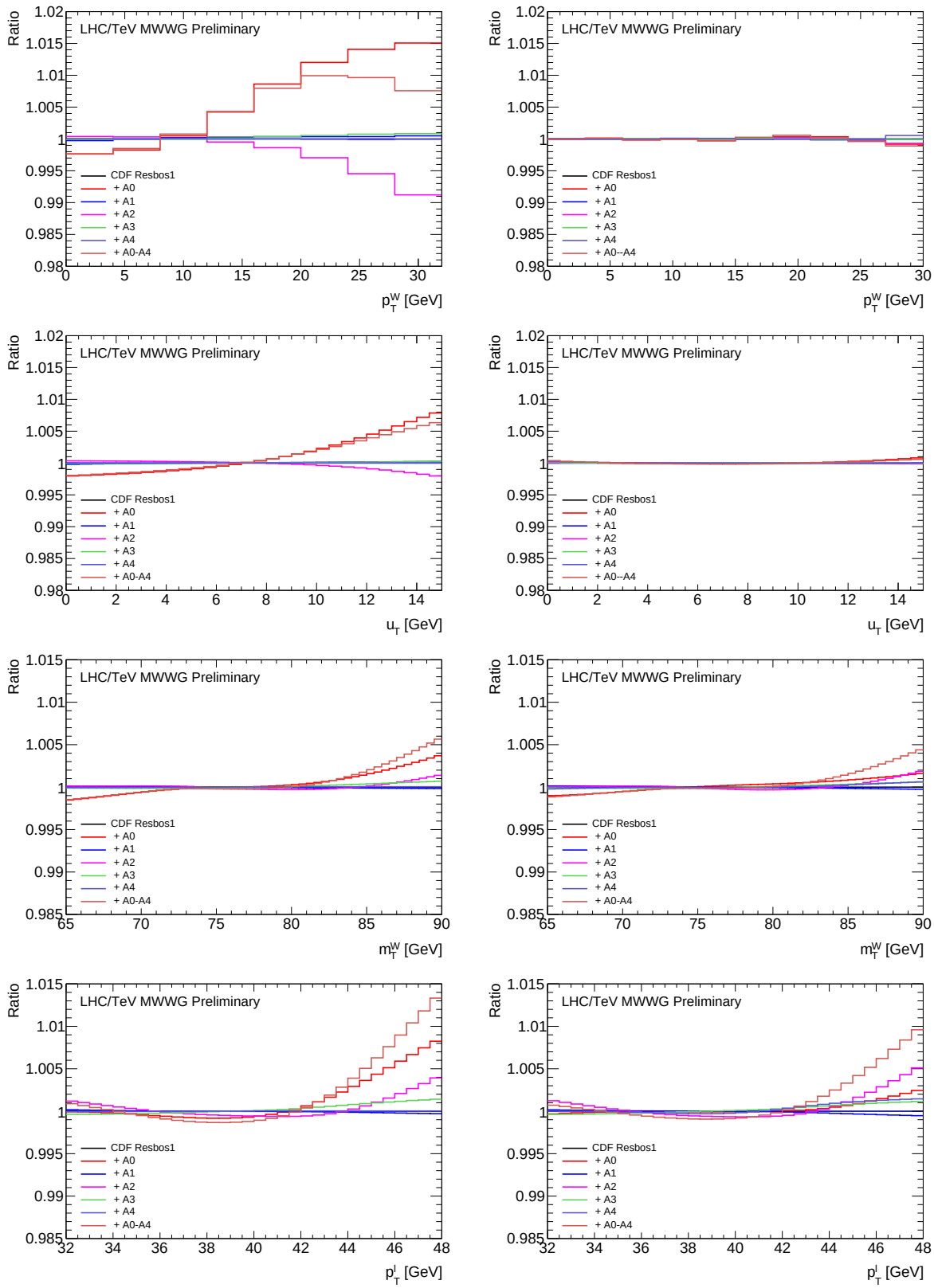

Figure 16: Relative effect of the $A_0 - A_4$ corrections on the final state distributions without (left) and with (right) p_{T}^W constraint, for CDF. From top to bottom : generator-level p_{T}^W distribution, after analysis cuts; detector-level p_{T}^W distribution; m_{T}; and p_{T}^ℓ. Ratios are calculated with respect to the CDF legacy distributions.

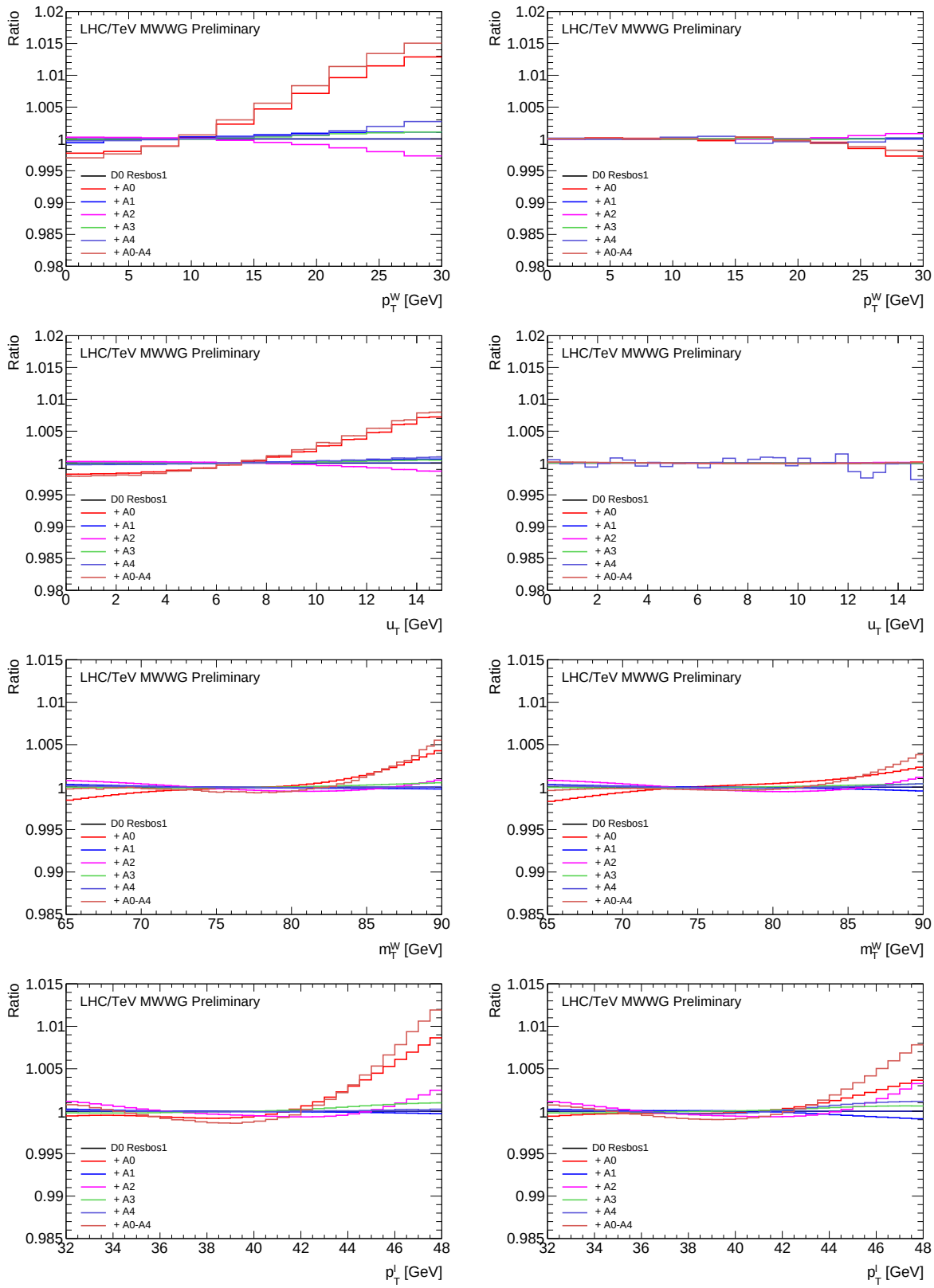

Figure 17: Relative effect of the $A_0 - A_4$ corrections on the final state distributions without (left) and with (right) p_T^W constraint, for D0. From top to bottom : generator-level p_T^W distribution, after analysis cuts; detector-level p_T^W distribution; m_T; and p_T^ℓ. Ratios are calculated with respect to the D0 legacy distributions.

reproduces the effect observed at high values of the kinematic distributions. Shifts of $\delta m_W^{\mathrm{QCD}} = 8$, 7 and 16 MeV are observed for the m_{T}, p_{T}^{ℓ} and p_{T}^{ν} distributions respectively. Since $\delta m_W^{\mathrm{QCD}}$ is positive, this implies downwards shifts for the measured values according to Eq. 3.

The numbers reported above reflect the improved treatment of spin correlations in ResBos2, compared to earlier versions of ResBos. The effects are larger than those found in Ref. [50], which evaluates the effect of perturbative improvements within ResBos2.

Correction	$\delta m_W^{\mathrm{QCD}}$ [MeV]					
	p_{T}^W-constrained			No constraint		
	p_{T}^{ℓ}	m_{T}	p_{T}^{ν}	p_{T}^{ℓ}	m_{T}	p_{T}^{ν}
Invariant mass	< 0.1	< 0.1	< 0.1	< 0.1	< 0.1	< 0.1
Rapidity	< 0.1	< 0.1	< 0.1	< 0.1	< 0.1	< 0.1
A_0	7.6	10.0	15.8	16.0	12.6	19.5
A_1	-2.4	-1.9	-1.8	-1.2	-1.6	-1.4
A_2	-3.0	-2.6	2.9	-4.2	-3.0	2.3
A_3	2.9	1.6	-0.5	3.5	1.8	-0.2
A_4	2.4	-0.1	-0.5	0.1	-0.7	-1.0
$A_0 - A_4$	7.6	7.0	16.0	14.1	9.1	18.9
Total	7.6	7.0	16.0	14.1	9.1	18.9
ResBos2	7.3±1.1	8.4±1.0	16.6±1.2	13.9±1.1	10.3±1.0	19.8±1.2
Non-closure	-0.3±1.1	1.4±1.0	0.6±1.2	-0.2±1.1	1.2±1.0	0.9±1.2

Table 5: Effect of reweighting the angular coefficients in the D0 ResBos1 events to those of ResBos2, as well as a direct fit of ResBos1 to ResBos2. Good closure is observed.

The analogous comparison for the CDF measurement is shown in Figure 19, while the m_W shifts are not reported pending the validation of the detector emulation.

6.4 Spin correlation effects : summary

The angular coefficients of W and Z production in ResBos1 differ from more recent calculations, and a method is proposed to bring the final state distributions in agreement with state-of-the-art predictions. The impact of this improvement is evaluated for the D0 measurements of m_W under two assumptions:

- constraining the selected p_{T}^W distribution to stay unchanged under the spin correlation corrections yields shifts of (7.3±1.1) and (8.4±1.0) for the p_{T}^{ℓ} and m_{T} fits in D0. This approach is justified by the satisfactory description of the selected u_{T} distributions, which results from the fit of the selected p_{T}^Z distribution to the data. This assumption however ignores the residual freedom of the underlying p_{T}^W distribution, and therefore under-estimates the effects.
- not constraining the selected p_{T}^W distribution yields shifts of (13.9±1.1) and (10.3±1.0) for the p_{T}^{ℓ} and m_{T} fits in D0. These numbers constitute an upper bound of the effect.

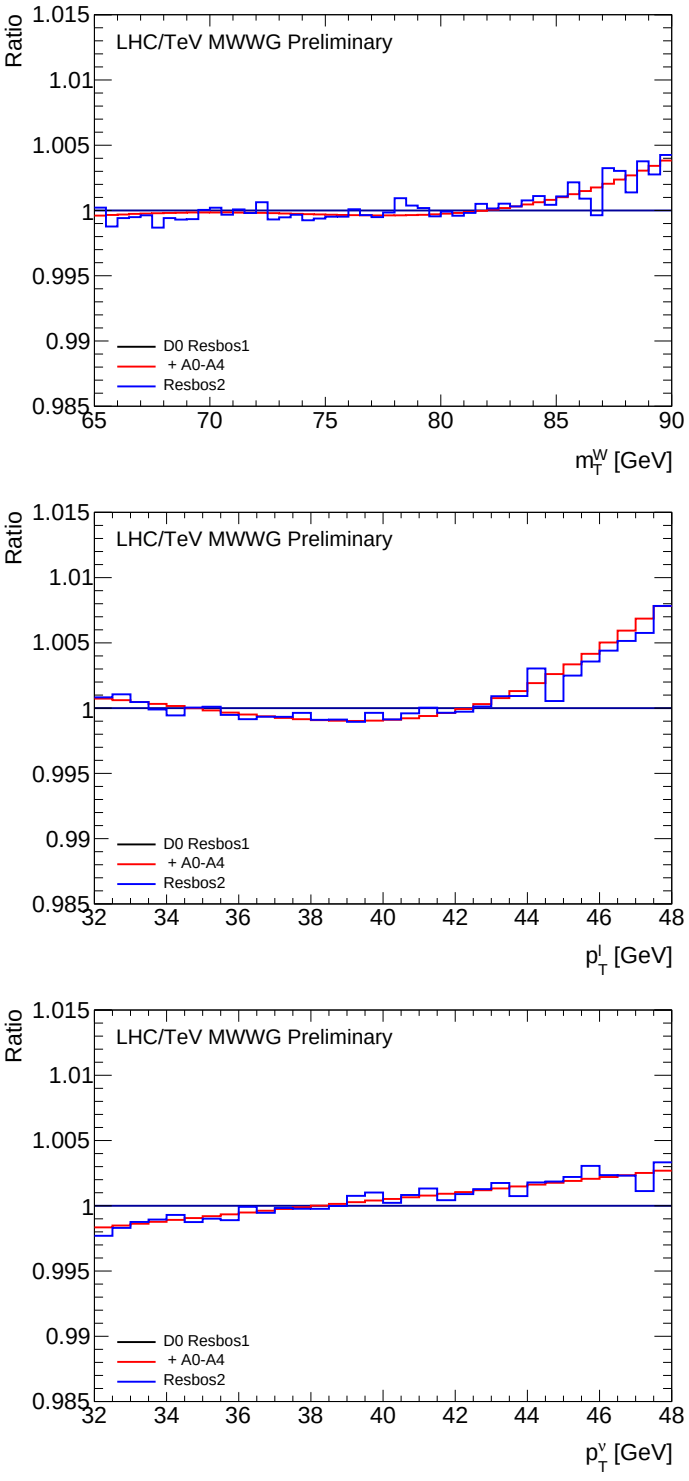

Figure 18: Relative effect of the generator corrections and comparison to RESBOS2 for D0, including the detector emulation and after applying the p_T^W constraint. Left : m_T distribution; right : p_T^ℓ distribution. Ratios are calculated with respect to the D0 legacy distributions.

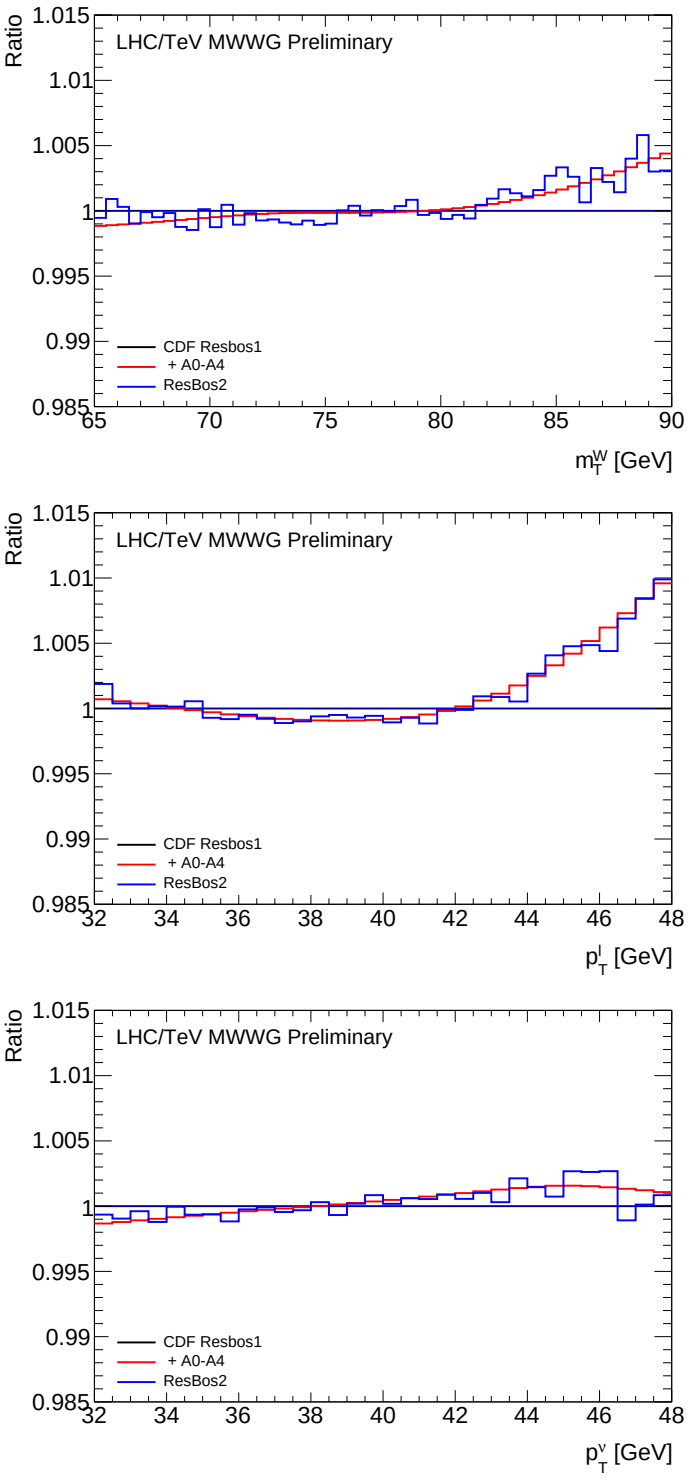

Figure 19: Relative effect of the generator corrections and comparison to ResBos2, for CDF, applying the p_T^W constraint. Left : m_T distribution; right : p_T^ℓ distribution. Ratios are calculated with respect to the CDF legacy distributions.

The numerical differences between the two approaches are moderate, and could be used to define a quantitative correction and its associated uncertainty. A more refined treatment would involve a study of the relative effect of spin corrections on the p_{T}^{W} and p_{T}^{Z} distributions.

7 PDF extrapolations

This section presents the methodology proposed for the extrapolations of published measurements of m_W to modern PDF sets, as well as the estimation of the corresponding uncertainty and correlations. This method is foreseen to be used for the measurement combination currently in preparation.

7.1 Updating existing measurements to alternate PDFs

Denoting $m_W^{\text{published}}$ the result of a published measurement performed using a reference PDF set, and m_W^{updated} the result corrected to an alternate PDF set, the latter can be written

$$m_W^{\text{updated}} = m_W^{\text{published}} - \delta m_W^{\text{PDF}} \tag{21}$$

where δm_W^{PDF} is introduced in Section 4 and defined with respect to the reference PDF set. Published values are always used for $m_W^{\text{published}}$; the measurement emulation procedure is only used for δm_W^{PDF}.

At CDF and D0, the low pile-up and centre-of-mass energy allow a measurement of the recoil, u_{T}, with a good experimental resolution. The u_{T} distribution probes the p_{T}^{W} distribution at detector level and, after tuning the non-perturbative parameters in Resbos1 using Z-boson data, achieves good agreement between data and simulation. The PDF extrapolations are thus performed under the constraint that the p_{T}^{W} distribution of selected W-boson events remains unchanged, by applying an additional event weight as

$$w_{\text{PDF}}^{\text{corr}}(p_{\mathrm{T}}^{W}) \equiv \left(\frac{1}{\sigma_W}\frac{d\sigma_W}{dp_{\mathrm{T}}}\right)_{\text{published}} \Bigg/ \left(\frac{1}{\sigma_W}\frac{d\sigma_W}{dp_{\mathrm{T}}}\right)_{\text{PDF}} \tag{22}$$

where the numerator is defined from the fiducial p_{T}^{W} distributions used for the corresponding publications, and shown in Figure 1. As for the spin correlations, this ansatz assumes any modification of the p_{T}^{W} distribution due to PDFs would be corrected in the fit to the Z data for the parameters describing the p_{T}^{W} and p_{T}^{Z} distributions. A more careful evaluation of these effects is beyond the scope of this document.

In the case of ATLAS, where the enhanced pile-up and underlying event induce a poorer recoil resolution, the detector-level u_{T} distribution does not significantly constrain the p_{T}^{W} distribution; the measurement however accounts for the precisely measured Z-boson p_{T} distribution at 7 TeV [73]. A weaker form of this constraint is thus applied, namely

$$w_{\text{PDF}}^{\text{corr}}(p_{\mathrm{T}}^{W}) \equiv \left(\frac{1}{\sigma_Z}\frac{d\sigma_Z}{dp_{\mathrm{T}}}\right)_{\text{published}} \Bigg/ \left(\frac{1}{\sigma_Z}\frac{d\sigma_Z}{dp_{\mathrm{T}}}\right)_{\text{PDF}} \tag{23}$$

which ensures that the Z-boson p_{T} distribution remains unchanged, and removes the part of the corresponding W-boson uncertainty that is correlated to the Z under PDF variations. This is approximately equivalent to

re-tuning the parton shower or resummation parameters to the Z data for each PDF variation, but simpler in practice.

7.2 PDF uncertainties

For Hessian PDF sets, the uncertainty corresponding to a given set is estimated as

$$\delta m_W^+ = \left[\sum_i \left(\delta m_W^i\right)^2\right]^{1/2} \text{ if } \delta m_W^i > 0, \qquad \delta m_W^- = \left[\sum_i \left(\delta m_W^i\right)^2\right]^{1/2} \text{ if } \delta m_W^i < 0, \tag{24}$$

where i runs over the uncertainty sets, and δm_W^i is the difference between the fitted value for set i and the reference PDF set. Only symmetrized uncertainties, $\delta m_W = (\delta m_W^+ + \delta m_W^-)/2$, are discussed below for simplicity. In the case of replica sets, obtained from fits to fluctuated data, a symmetric uncertainty is estimated from the spread of the fitted values of m_W over the N replicas:

$$\delta m_W = \left[\frac{1}{N}\sum_i \left(\delta m_W^i\right)^2\right]^{1/2}. \tag{25}$$

The effect of each PDF eigenset is fully correlated across experiment or measurement categories, and its contribution to the covariance between any two measurements α, β is given by

$$C_{\alpha\beta}^i = \delta m_{W\,\alpha}^i \delta m_{W\beta}^i. \tag{26}$$

Accounting for all eigensets of a given set, the total PDF uncertainty covariance and the corresponding uncertainty correlation are calculated as

$$C_{\alpha\beta}^{\text{PDF}} = \sum_i C_{\alpha\beta}^i, \quad \rho_{\alpha\beta} = \frac{\sum_i \delta m_{W\,\alpha}^i \delta m_{W\beta}^i}{\delta m_{W\,\alpha}\delta m_{W\beta}}. \tag{27}$$

These uncertainties and correlations are then used in the averaging, which is performed using BLUE [64]. The remaining PDF dependence of the result is evaluated by repeating the averaging procedure for an ensemble of representative PDF sets, selected by the quality of their description of the available Drell-Yan cross-section data.

8 Comparison of PDF predictions with global Drell-Yan data

Global PDF determinations from different PDF Collaborations make different choices of input data, use different theory predictions and a different parametrisation for the non-perturbative part. In the derivation of uncertainties ad-hoc tolerance criteria on the χ^2 are typically used to account for tensions between the experimental data and the predictions or between different datasets. Given their large dependence on the PDFs, it is important to ensure the PDFs used give a good description of the Drell-Yan data available in the (x, Q^2) range relevant for the TeVatron and ATLAS m_W measurements.

exp.	obs	channel	$\sqrt{s}$	lumi	pts	ref
CDF	A_W	$e\nu$	1.96 TeV	1 fb^{-1}	13	[82]
CDF	y_Z	ee	1.96 TeV	2.1 fb^{-1}	28	[83]
D0	y_Z	ee	1.96 TeV	0.4 fb^{-1}	28	[84]
D0	A_l	$\mu\nu$	1.96 TeV	7.3 fb^{-1}	12	[85]
D0	A_l	$e\nu$	1.96 TeV	9.7 fb^{-1}	13	[86]
ATLAS	Z,W	ll,$l\nu$	7 TeV	4.7 fb^{-1}	61	[87]

Table 6: W- and Z-boson cross-section measurements considered in this benchmarking. For each measurement the observable measured, the leptonic decay channel, the center-of-mass energy, integrated luminosity and number of data points are reported.

Dataset	CT10	cteq6	cteq66
CDF Z rapidity	29|33 / 28	33|29 / 28	31|32 / 28
CDF W asymmetry	14|22 / 13	14|21 / 13	16|18 / 13
D0 Z rapidity	22|22 / 28	22|22 / 28	22|22 / 28
D0 $We\nu$ lepton asymmetry	20|33 / 13	20|22 / 13	22|26 / 13
D0 $W\mu\nu$ lepton asymmetry	11|13 / 10	12|13 / 10	11|12 / 10
ATLAS peak CC Z rapidity	14|25 / 12	21|214 / 12	18|29 / 12
ATLAS W^- lepton rapidity	10|25 / 11	21|38 / 11	14|44 / 11
ATLAS W^+ lepton rapidity	11|28 / 11	12|59 / 11	12|59 / 11
Correlated χ^2	52|166	158|513	90|236
Log penalty χ^2	-3.94|-3.94	-7.70|-7.70	-4.37|-4.37
Total χ^2 / dof	179|364 / 126	306|923 / 126	231|472 / 126
χ^2 p-value	0.00	0.00	0.00

Table 7: Goodness-of-fit for the Tevatron 1.96 TeV and ATLAS 7 TeV Z and W cros-section measurements compared to NNLO QCD + NLO EW theory predictions with the PDF sets used in the W-mass measurements. The numbers before (after) the vertical bar "|" denote the χ^2 computed including (excluding) the PDF uncertainties. The PDF uncertainty corresponds to a 68% coverage, and is obtained by rescaling the eigenvectors by a factor 1/1.645.

In this Section, we benchmark different global PDF fits against Drell-Yan measurements from the TeVatron at 1.96 TeV and the ATLAS Collaborations at 7 TeV. The list of measurements considered is presented in Tab. 6. The comparison between data and predictions is done with the xFitter [74, 75] framework. A χ^2 measure is constructed including all experimental uncertainties and their correlations as well as the PDF uncertainties and is used to quantify the agreement between the theoretical predictions and the data. PDF uncertainties are computed at NLO in QCD using APPLgrids [76] generated using MCFM-6.8 [77]. The nominal theoretical predictions are produced at NNLO in QCD with the FEWZ code [70, 78] using the dilepton invariant mass as renormalization and factorization scales and the NNPDF31_nnlo_as_0118 PDF set. They are combined with multiplicative k-factors for NLO EW effects including the pure EW virtual corrections and the QED initial-state and initial-final interference effects calculated with the SANC [79–81] code.

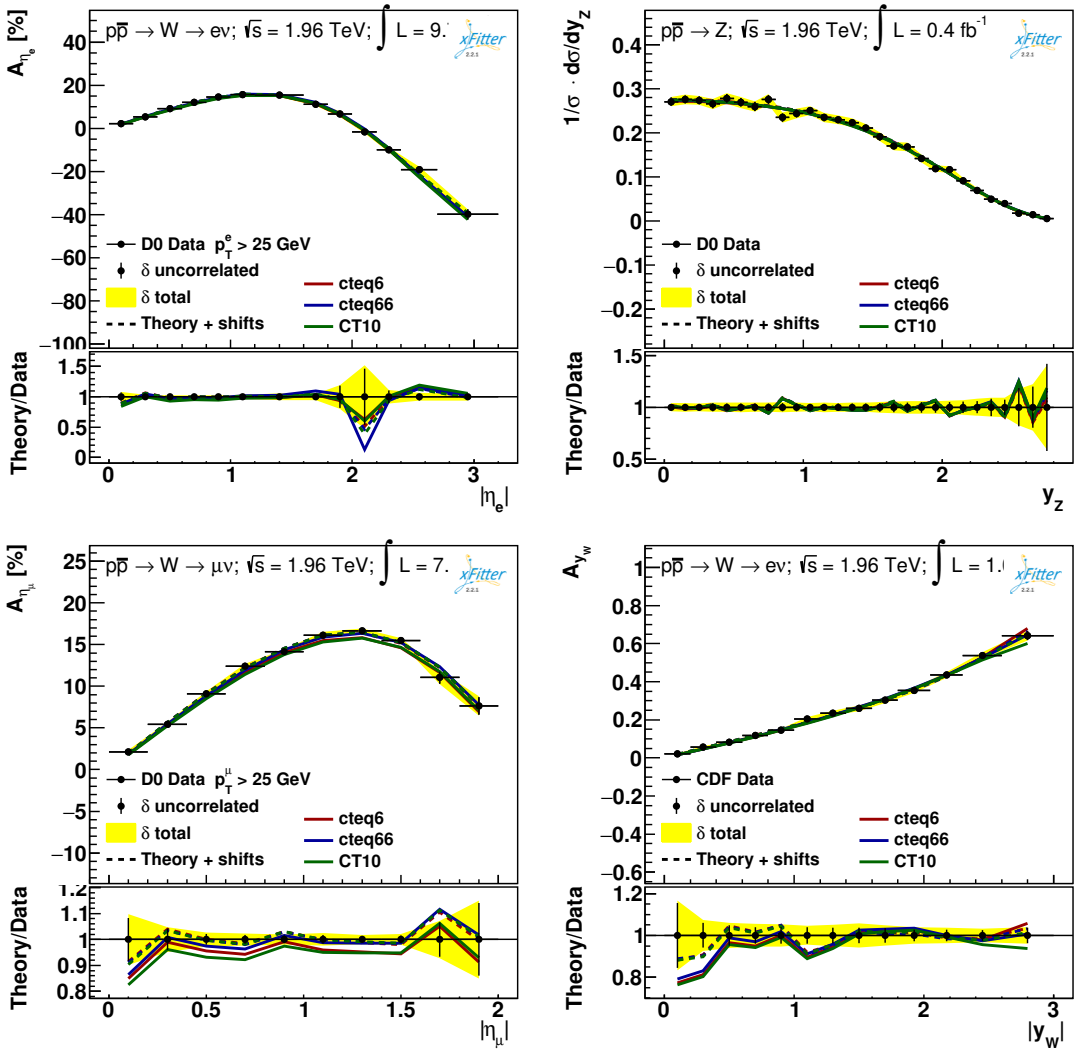

Figure 20: Comparison of the NNLO QCD+NLO EW theoretical predictions using different legacy PDF sets against measurements of the D0 W-boson electron (top left) and muon (bottom left) charge asymmetry, the D0 Z-boson rapidity (top right) and the CDF W-boson charge asymmetry (bottom right).

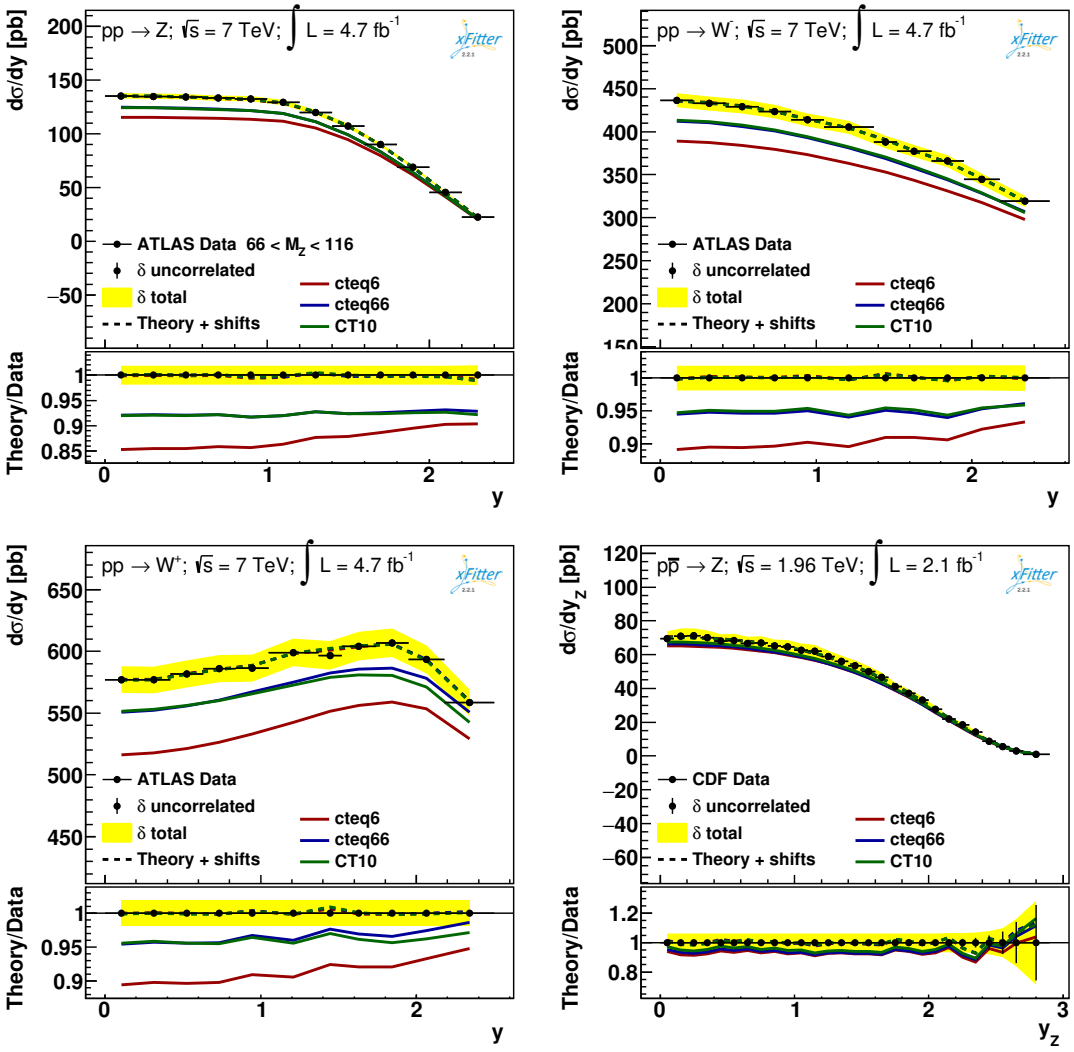

Figure 21: Comparison of the NNLO QCD+NLO EW theoretical predictions using different legacy PDF sets against measurements of the ATLAS Z-boson rapidity (top left), W^+ (bottom left) and W^- (top right) lepton rapidity and CDF Z-boson rapidity (bottom right) distributions.

Dataset	NNPDF31	NNPDF40	MMHT14	MSHT20	CT18NNLO	ABMP16
CDF Z rapidity	24|28 / 28	28|30 / 28	30|31 / 28	32|32 / 28	27|27 / 28	31|31 / 28
CDF W asymmetry	11|57 / 13	14|17 / 13	12|13 / 13	28|27 / 13	11|35 / 13	21|43 / 13
D0 Z rapidity	22|22 / 28	23|23 / 28	23|23 / 28	24|23 / 28	22|22 / 28	22|22 / 28
D0 $We\nu$ lepton asymmetry	22|32 / 13	23|29 / 13	52|51 / 13	42|40 / 13	19|32 / 13	26|24 / 13
D0 $W\mu\nu$ lepton asymmetry	12|14 / 10	12|16 / 10	11|14 / 10	11|13 / 10	12|13 / 10	11|12 / 10
ATLAS peak CC Z rapidity	13|18 / 12	13|17 / 12	58|89 / 12	17|19 / 12	11|77 / 12	18|32 / 12
ATLAS W^- lepton rapidity	12|18 / 11	12|15 / 11	33|33 / 11	16|17 / 11	9.9|28 / 11	14|17 / 11
ATLAS W^+ lepton rapidity	8.9|13 / 11	8.6|11 / 11	15|21 / 11	12|13 / 11	9.4|16 / 11	10|12 / 11
Correlated χ^2	76|110	63|83	212|236	91|102	43|251	86|108
Log penalty χ^2	-0.62|-0.62	-0.58|-0.58	-1.62|-1.62	-2.89|-2.89	-1.68|-1.68	-2.72|-2.72
Total χ^2 / dof	200|312 / 126	195|242 / 126	445|509 / 126	270|283 / 126	163|499 / 126	236|300 / 126
χ^2 p-value	0.00	0.00	0.00	0.00	0.02	0.00

Table 8: Goodness-of-fit for the Tevatron 1.96 TeV and ATLAS 7 TeV Z and W cros-section measurements compared to NNLO QCD + NLO EW theory predictions using different modern global PDF sets. The numbers before (after) the vertical bar "|" denote the χ^2 computed including (excluding) the PDF uncertainties. The CTEQ PDFs uncertainty corresponds to a 68% coverage, and is obtained by rescaling the eigenvectors by a factor 1/1.645.

Dataset	CT18ANNLO	CT18ZNNLO	CT18XNNLO	CT14nnlo	CT10nnlo	CJ15nlo
CDF Z rapidity	28|29 / 28	28|29 / 28	28|27 / 28	29|29 / 28	29|28 / 28	32|30 / 28
CDF W asymmetry	12|30 / 13	12|28 / 13	11|33 / 13	12|28 / 13	16|34 / 13	21|27 / 13
D0 Z rapidity	22|22 / 28	22|23 / 28	22|22 / 28	22|22 / 28	22|22 / 28	23|22 / 28
D0 $We\nu$ lepton asymmetry	21|33 / 13	21|29 / 13	21|31 / 13	20|32 / 13	24|69 / 13	39|49 / 13
D0 $W\mu\nu$ lepton asymmetry	11|12 / 10	11|12 / 10	11|13 / 10	11|13 / 10	11|18 / 10	17|26 / 10
ATLAS peak CC Z rapidity	10|19 / 12	9.7|21 / 12	12|71 / 12	13|42 / 12	12|27 / 12	60|104 / 12
ATLAS W^- lepton rapidity	10|17 / 11	10|17 / 11	13|27 / 11	11|27 / 11	10|41 / 11	23|27 / 11
ATLAS W^+ lepton rapidity	8.7|10 / 11	8.1|9.5 / 11	8.9|15 / 11	9.3|12 / 11	9.6|43 / 11	14|15 / 11
Correlated χ^2	49|113	43|113	82|230	63|175	58|198	269|314
Log penalty χ^2	-1.69|-1.69	-0.33|-0.33	-1.05|-1.05	-2.04|-2.04	-1.51|-1.51	-5.38|-5.38
Total χ^2 / dof	170|284 / 126	165|280 / 126	209|468 / 126	187|376 / 126	190|478 / 126	492|610 / 126
χ^2 p-value	0.01	0.01	0.00	0.00	0.00	0.00

Table 9: Goodness-of-fit for the Tevatron 1.96 TeV and ATLAS 7 TeV Z and W cros-section measurements compared to NNLO QCD + NLO EW theory predictions using different global PDF sets by the CTEQ Collaboration. The numbers before (after) the vertical bar "|" denote the χ^2 computed including (excluding) the PDF uncertainties. The CTEQ PDFs uncertainty corresponds to a 68% coverage, and is obtained by rescaling the eigenvectors by a factor 1/1.645.

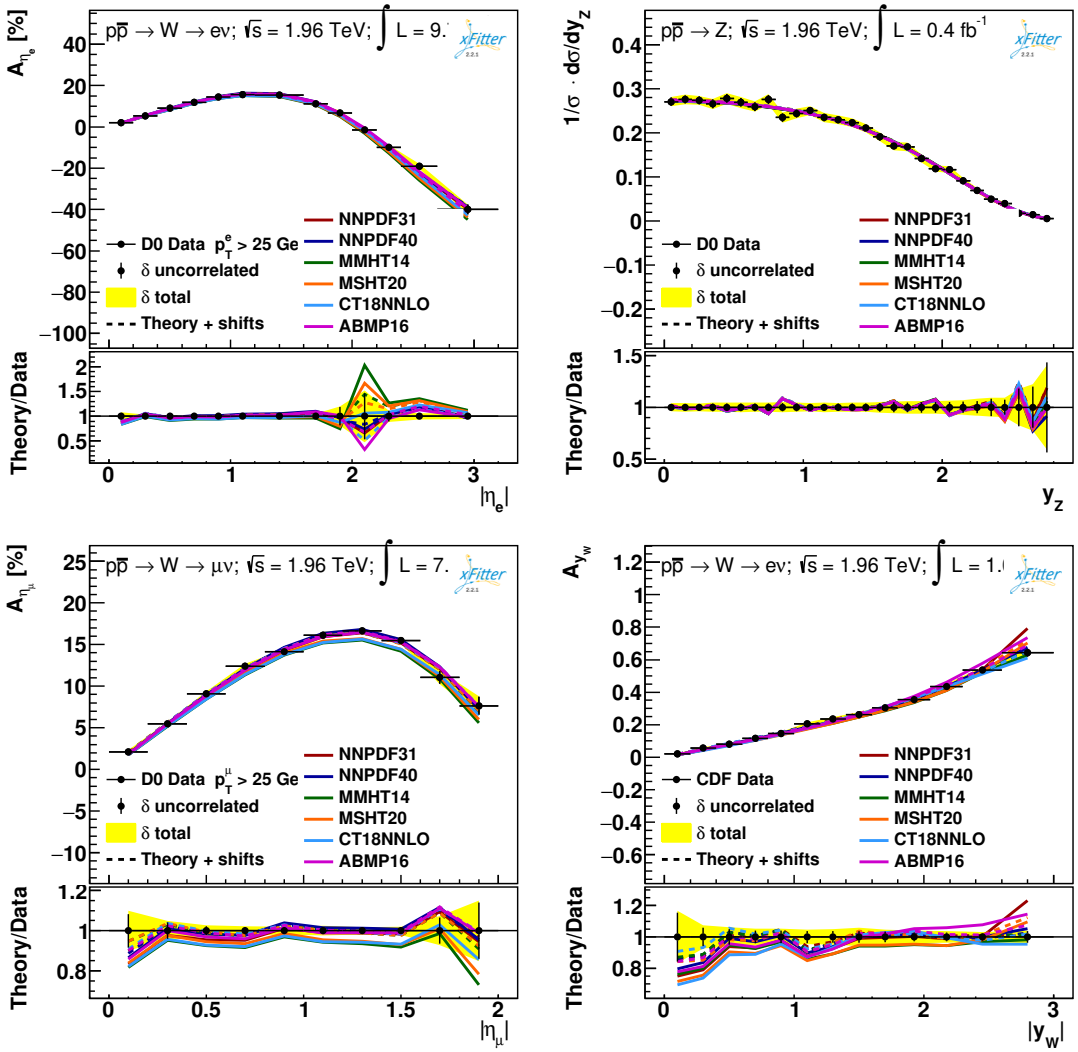

Figure 22: Comparison of the NNLO QCD+NLO EW theoretical predictions using different modern PDFs against measurements of the D0 W-boson electron (top left) and muon (bottom left) charge asymmetry, the D0 Z-boson rapidity (top right) and the CDF W-boson charge asymmetry (bottom right).

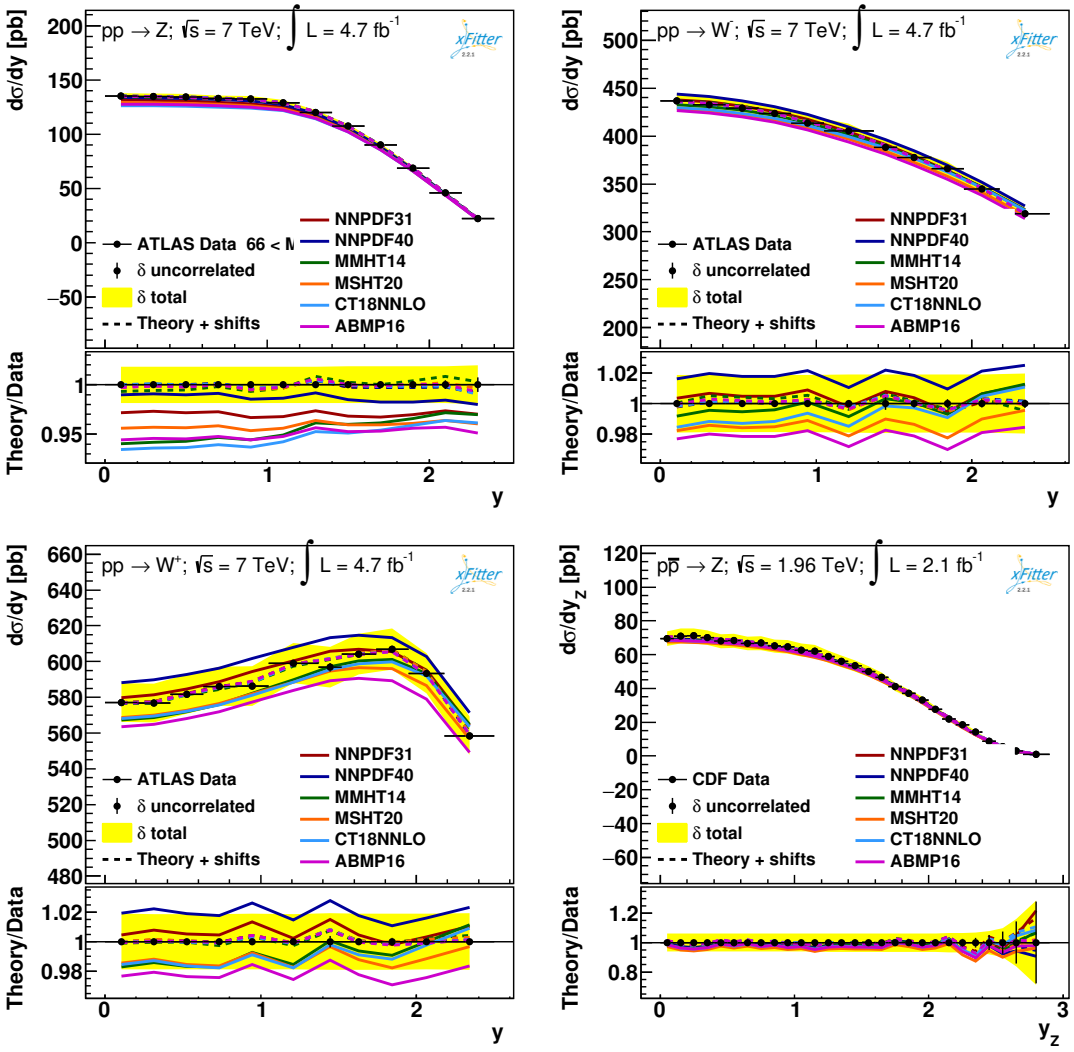

Figure 23: Comparison of the NNLO QCD+NLO EW theoretical predictions using different modern PDF sets against measurements of the ATLAS Z-boson rapidity (top left), W^+ (bottom left) and W^- (top right) lepton rapidity and CDF Z-boson rapidity (bottom right) distributions.

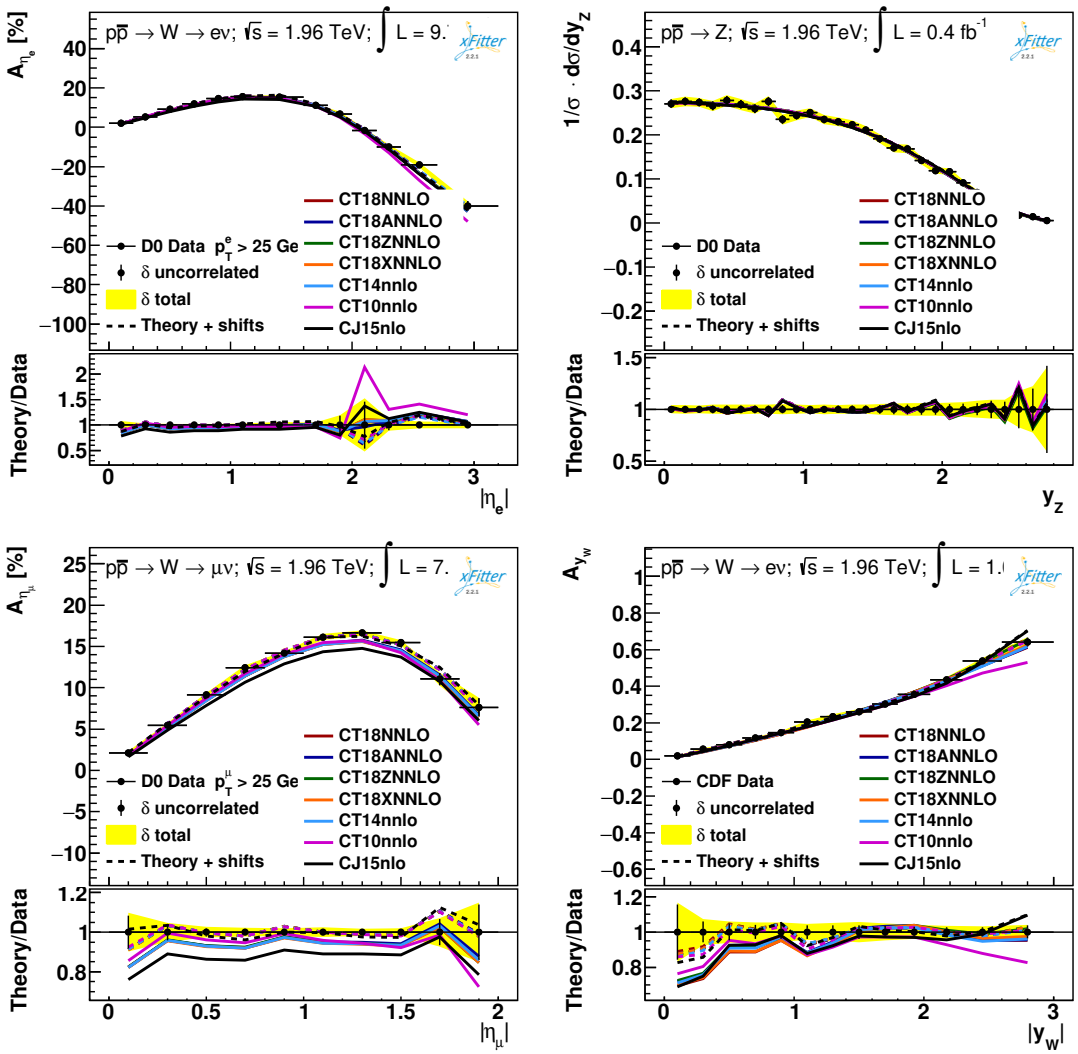

Figure 24: Comparison of the NNLO QCD+NLO EW theoretical predictions using different different PDF sets from the CTEQ Collaboration against measurements of the D0 W-boson electron (top left) and muon (bottom left) charge asymmetry, the D0 Z-boson rapidity (top right) and the CDF W-boson charge asymmetry (bottom right).

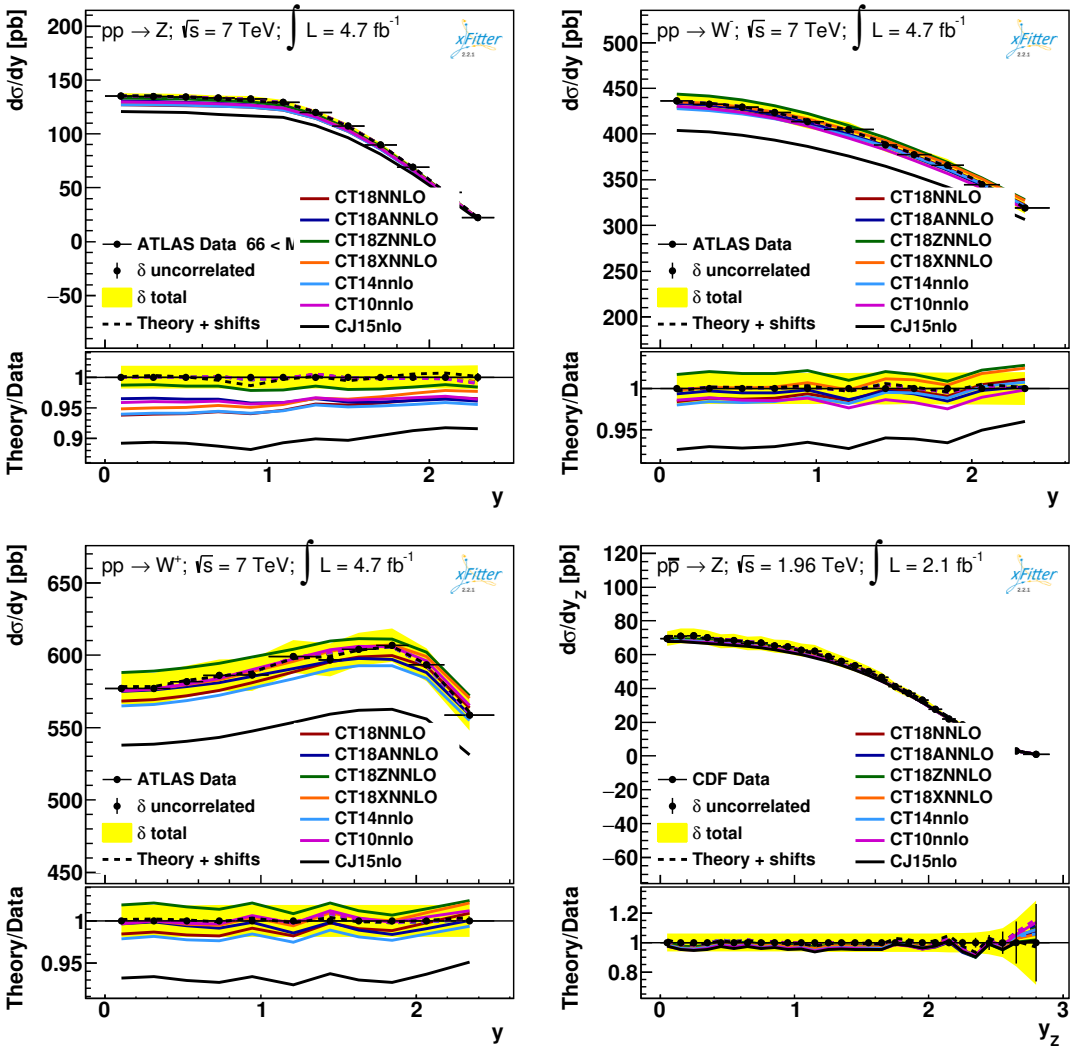

Figure 25: Comparison of the NNLO QCD+NLO EW theoretical predictions using different PDF sets from the CTEQ Collaboration against measurements of the ATLAS Z-boson rapidity (top left), W^+ (bottom left) and W^- (top right) lepton rapidity and CDF Z-boson rapidity (bottom right) distributions.

The first set of PDFs considered are the ones used in the original W-mass measurements: cteq6 [29] for CDF, cteq66 [21] for D0 and CT10 [31] for ATLAS. Their description of Drell-Yan cross-sections is reported in Tab. 7. For each measurement the partial $\chi 2$ is reported including or excluding the PDF uncertainties form the predictions. The "Correlated χ^2" indicates the contribution from bin-by-bin systematic correlations in the measurements data, while the "Log penalty χ^2" arises from the likelihood transition to χ^2 when the errors scaling is applied [88]. Finally, the "Total χ^2" is reported with its corresponding probability (p-value). The agreement between the theoretical predictions using different PDFs and the data is shown in Fig. 20 and 21.

In a second set of comparisons, presented in Tab. 8 and Figs. 22, 23 the more modern global PDF determinations are considered. These are the NNPDF31_nnlo_as_0118 [37] and NNPDF40_nnlo_as_01180 [37], the MMHT2014nnlo68cl [36] and MSHT20nnlo_as118 [15], the CT18NNLO [14] and the ABMP16_5_nnlo [38].

The last comparison, shown in Tab. 9 and Figs. 24,25 involves several PDFs from the CTEQ-TEA Collaboration; the older sets CT10nnlo [32], CT14nnlo [33] and CJ15nlo [39], as well as the variations of the CT18NNLO [14] fit: X, A and Z. As the eigenvectors for these PDFs are reported for a 90% CL, to recover a 68% CL their eigenvectors are rescaled by a factor 1/1.645.

None of the PDF sets considered are found to provide an overall good description of the data, with χ^2/dof significantly larger than one giving very small probabilities. This is a known fact, which can be partly attributed to the lack of theoretical uncertainties in the χ^2 definition (both the one used in the PDF extraction and the one used in this benchmarking), and partly to known issues in the theoretical accuracy of the fixed-order QCD predictions when describing fiducial measurements [89, 90]. On this latter point, we note that for both the Tevatron and LHC m_W measurements the predictions used to model the W kinematic include the effect of q_T resummation (analytic in the case of Resbos, or through a Monte Carlo approach for Pythia). The resummation on the one hand should cure the issue of accuracy of the predictions after fiducial selections, and on the other will introduce a mismatch between the fixed-order predictions used to extract PDFs and the resummed predictions used determine m_W.

Among the legacy sets the CT10 PDF is found to provide the best description of these measurements, with a total χ^2 not worse than that of modern determinations. Of the modern PDF sets, the CT18NNLO and NNPDF40 fits provide the best χ^2, followed by the ABMP16 and MSHT20 sets. The CT18X, Z, A sets do not improve over the nominal fit, despite the inclusion of the ATLAS W, Z data in the A and Z variations.

All modern global PDF determinations; NNPDF3.1, CT18NNLO, MSHT20, ABMP16 and the recent NNPDF4.0 PDF are found to provide satisfactory descriptions of the relevant experimental data, and as such should be considered for the purpose of the combination of m_W measurements. We note that the χ^2 of the m_W combination itself is also expected to provide some discriminating power on the PDFs.

9 Conclusion

We presented a study of physics modelling and PDF correlation effects towards a combination of the ATLAS, CDF and D0 measurements of the W-boson mass.

The measurement correlations are dominated by uncertainties in the PDFs, for which different choices have been made. A benchmarking of fixed-order NNLO QCD+NLO EW predictions using a wide set of PDF determinations showed how modern global PDF determinations at NNLO QCD provide a significantly

improved description of W- and Z-boson cross-section measurements from the TeVatron and LHC over the PDF fits used in the original publications.

The different modelling assumptions for the W-boson production and decay also motivate an update of past measurements in view of the progress in perturbative QCD calculations over the past years. In particular, extensive comparisons against state-of-the-art QCD predictions highlighted the need to correct the TeVatron W-boson mass determinations for the treatment of lepton angular distributions in W-boson decay in the legacy Resbos codes. In the context of the D0 measurement, correcting the spin correlations affects the result at the level of -10 MeV, depending on the distribution used in the fit.

In summary, methods are presented to evaluate the effect of improved QCD predictions and PDF variations on existing measurement results in a realistic way, which allows extrapolating past measurements to any past or present PDF set and evaluate the corresponding uncertainties. Based on this method, the measurements can be corrected to a set of common PDF references, and combined accounting for the partial PDF correlations in a quantitative way.

10 Acknowledgements

We are glad to thank Joshua Isaacson, Pavel Nadolsky, Frank Tackmann and C.-P. Yuan for fruitful discussions. We are grateful to Joshua Isaacson and Yao Fu for providing us with the necessary inputs for event generation with RESBOS2. We are indebted to colleagues from the TeVatron and LHC collaborations for their careful reading and feedback on this note.

References

[1] CDF Collaboration, *High-precision measurement of the W boson mass with the CDF II detector*, Science **376** (2022) 170 (cit. on pp. 3, 5, 12).

[2] D0 Collaboration, *Measurement of the W boson mass*, Phys. Rev. Lett. **103** (2009) 141801, arXiv: 0908.0766 [hep-ex] (cit. on p. 3).

[3] D0 Collaboration, *Measurement of the W boson mass with the D0 detector*, Phys. Rev. **D89** (2014) 012005, arXiv: 1310.8628 [hep-ex] (cit. on pp. 3, 6, 13–15).

[4] ATLAS Collaboration, *Measurement of the W-boson mass in pp collisions at $\sqrt{s}$ = 7 TeV with the ATLAS detector*, Eur. Phys. J. **C78** (2018) 110, [Erratum: Eur. Phys. J.C78,no.11,898(2018)], arXiv: 1701.07240 [hep-ex] (cit. on pp. 3, 17, 26).

[5] LHCb Collaboration, *Measurement of the W boson mass*, JHEP **01** (2022) 036, arXiv: 2109.01113 [hep-ex] (cit. on pp. 3, 26).

[6] S. Dittmaier and M. Krämer, *Electroweak radiative corrections to W boson production at hadron colliders*, Phys. Rev. D **65** (2002) 073007, arXiv: hep-ph/0109062 (cit. on p. 3).

[7] C. Duhr, F. Dulat and B. Mistlberger, *Charged current Drell-Yan production at N^3LO*, JHEP **11** (2020) 143, arXiv: 2007.13313 [hep-ph] (cit. on p. 3).

[8] X. Chen et al., *Transverse Mass Distribution and Charge Asymmetry in W Boson Production to Third Order in QCD*, (2022), arXiv: 2205.11426 [hep-ph] (cit. on p. 3).

[9] S. Dittmaier, A. Huss and C. Schwinn, *Dominant mixed QCD-electroweak $O(\alpha_s\alpha)$ corrections to Drell–Yan processes in the resonance region*, Nucl. Phys. B **904** (2016) 216, arXiv: 1511.08016 [hep-ph] (cit. on p. 3).

[10] A. Behring et al., *Mixed QCD-electroweak corrections to W-boson production in hadron collisions*, Phys. Rev. D **103** (2021) 013008, arXiv: 2009.10386 [hep-ph] (cit. on p. 3).

[11] L. Buonocore, M. Grazzini, S. Kallweit, C. Savoini and F. Tramontano, *Mixed QCD-EW corrections to $pp \to \ell\nu_\ell + X$ at the LHC*, Phys. Rev. D **103** (2021) 114012, arXiv: 2102.12539 [hep-ph] (cit. on p. 3).

[12] A. Behring et al., *Estimating the impact of mixed QCD-electroweak corrections on the W-mass determination at the LHC*, Phys. Rev. D **103** (2021) 113002, arXiv: 2103.02671 [hep-ph] (cit. on p. 3).

[13] M. Pellen, R. Poncelet, A. Popescu and T. Vitos, *Angular coefficients in W+j production at the LHC with high precision*, (2022), arXiv: 2204.12394 [hep-ph] (cit. on p. 3).

[14] T.-J. Hou et al., *New CTEQ global analysis of quantum chromodynamics with high-precision data from the LHC*, (2019), arXiv: 1912.10053 [hep-ph] (cit. on pp. 3, 42).

[15] S. Bailey, T. Cridge, L. A. Harland-Lang, A. D. Martin and R. S. Thorne, *Parton distributions from LHC, HERA, Tevatron and fixed target data: MSHT20 PDFs*, Eur. Phys. J. C **81** (2021) 341, arXiv: 2012.04684 [hep-ph] (cit. on pp. 3, 5, 42).

[16] R. D. Ball et al., *The Path to Proton Structure at One-Percent Accuracy*, (2021), arXiv: 2109.02653 [hep-ph] (cit. on pp. 3, 5).

[17] CDF Collaboration, *Precise measurement of the W-boson mass with the CDF II detector*, Phys. Rev. Lett. **108** (2012) 151803, arXiv: 1203.0275 [hep-ex] (cit. on p. 3).

[18] CDF Collaboration, *Precise measurement of the W-boson mass with the Collider Detector at Fermilab*, Phys. Rev. **D89** (2014) 072003, arXiv: 1311.0894 [hep-ex] (cit. on pp. 3, 12, 13).

[19] G. A. Ladinsky and C. P. Yuan, *The Nonperturbative regime in QCD resummation for gauge boson production at hadron colliders*, Phys. Rev. **D50** (1994) R4239, arXiv: hep-ph/9311341 [hep-ph] (cit. on p. 3).

[20] T. Sjostrand, S. Mrenna and P. Z. Skands, *PYTHIA 6.4 Physics and Manual*, JHEP **05** (2006) 026, arXiv: hep-ph/0603175 (cit. on p. 3).

[21] P. M. Nadolsky et al., *Implications of CTEQ global analysis for collider observables*, Phys. Rev. D **78** (2008) 013004, arXiv: 0802.0007 [hep-ph] (cit. on pp. 3, 5, 42).

[22] C. Balazs and C. P. Yuan, *Soft gluon effects on lepton pairs at hadron colliders*, Phys. Rev. **D56** (1997) 5558, arXiv: hep-ph/9704258 [hep-ph] (cit. on pp. 3, 6).

[23] F. Landry, R. Brock, P. M. Nadolsky and C. P. Yuan, *Tevatron Run-1 Z boson data and Collins-Soper-Sterman resummation formalism*, Phys. Rev. **D67** (2003) 073016, arXiv: hep-ph/0212159 [hep-ph] (cit. on pp. 3, 6).

[24] T. Sjöstrand et al., *An Introduction to PYTHIA 8.2*, Comput. Phys. Commun. **191** (2015) 159, arXiv: 1410.3012 [hep-ph] (cit. on p. 4).

[25] J. de Blas et al., *The Global Electroweak and Higgs Fits in the LHC era*, PoS **EPS-HEP2017** (2017) 467, arXiv: 1710.05402 [hep-ph] (cit. on p. 4).

[26] J. Haller et al., *Update of the global electroweak fit and constraints on two-Higgs-doublet models*, Eur. Phys. J. **C78** (2018) 675, arXiv: 1803.01853 [hep-ph] (cit. on p. 4).

[27] M. Tanabashi et al., *Review of Particle Physics*, Phys. Rev. **D98** (2018) 030001 (cit. on p. 4).

[28] P. Azzi et al., *Report from Working Group 1: Standard Model Physics at the HL-LHC and HE-LHC*, CERN Yellow Rep. Monogr. **7** (2019) 1, ed. by A. Dainese et al., arXiv: 1902.04070 [hep-ph] (cit. on p. 4).

[29] J. Pumplin et al., *New generation of parton distributions with uncertainties from global QCD analysis*, JHEP **07** (2002) 012, arXiv: hep-ph/0201195 (cit. on pp. 5, 42).

[30] D. Stump et al., *Inclusive jet production, parton distributions, and the search for new physics*, JHEP **10** (2003) 046, arXiv: hep-ph/0303013 [hep-ph] (cit. on p. 5).

[31] H.-L. Lai, M. Guzzi, J. Huston, Z. Li, P. M. Nadolsky et al., *New parton distributions for collider physics*, Phys. Rev. D **82** (2010) 074024, arXiv: 1007.2241 [hep-ph] (cit. on pp. 5, 42).

[32] J. Gao et al., *CT10 next-to-next-to-leading order global analysis of QCD*, Phys. Rev. **D89** (2014) 033009, arXiv: 1302.6246 [hep-ph] (cit. on pp. 5, 42).

[33] S. Dulat et al., *New parton distribution functions from a global analysis of quantum chromodynamics*, Phys. Rev. D **93** (2016) 033006, arXiv: 1506.07443 [hep-ph] (cit. on pp. 5, 42).

[34] T.-J. Hou et al., *Progress in the CTEQ-TEA NNLO global QCD analysis*, (2019), arXiv: 1908.11394 [hep-ph] (cit. on p. 5).

[35] A. D. Martin, W. J. Stirling, R. S. Thorne, and G. Watt, *Parton distributions for the LHC*, Eur. Phys. J. C **63** (2009) 189, arXiv: 0901.0002 [hep-ph] (cit. on p. 5).

[36] L. A. Harland-Lang, A. D. Martin, P. Motylinski and R. S. Thorne, *Parton distributions in the LHC era: MMHT 2014 PDFs*, Eur. Phys. J. C **75** (2015) 204, arXiv: 1412.3989 [hep-ph] (cit. on pp. 5, 42).

[37] R. D. Ball et al., *Parton distributions from high-precision collider data*, Eur. Phys. J. C **77** (2017) 663, arXiv: 1706.00428 [hep-ph] (cit. on pp. 5, 42).

[38] S. Alekhin, J. Blümlein, S. Moch and R. Placakyte, *Parton distribution functions, α_s, and heavy-quark masses for LHC Run II*, Phys. Rev. D **96** (2017) 014011, arXiv: 1701.05838 [hep-ph] (cit. on pp. 5, 42).

[39] A. Accardi, L. T. Brady, W. Melnitchouk, J. F. Owens and N. Sato, *Constraints on large-x parton distributions from new weak boson production and deep-inelastic scattering data*, Phys. Rev. D **93** (2016) 114017, arXiv: 1602.03154 [hep-ph] (cit. on pp. 5, 42).

[40] N. Davidson, T. Przedzinski and Z. Was, *PHOTOS Interface in C++: Technical and Physics Documentation*, Comput. Phys. Commun. **199** (2016) 86, arXiv: 1011.0937 [hep-ph] (cit. on p. 5).

[41] L. Barze, G. Montagna, P. Nason, O. Nicrosini and F. Piccinini, *Implementation of electroweak corrections in the POWHEG BOX: single W production*, JHEP **04** (2012) 037, arXiv: 1202.0465 [hep-ph] (cit. on p. 5).

[42] L. Barze et al., *Neutral current Drell-Yan with combined QCD and electroweak corrections in the POWHEG BOX*, Eur. Phys. J. C **73** (2013) 2474, arXiv: 1302.4606 [hep-ph] (cit. on p. 5).

[43] P. Nason, *A new method for combining NLO QCD with shower Monte Carlo algorithms*, JHEP **11** (2004) 040, arXiv: hep-ph/0409146 (cit. on p. 5).

[44] S. Frixione, P. Nason and C. Oleari, *Matching NLO QCD computations with parton shower simulations: the POWHEG method*, JHEP **11** (2007) 070, arXiv: 0709.2092 [hep-ph] (cit. on p. 5).

[45] S. Alioli, P. Nason, C. Oleari and E. Re, *A general framework for implementing NLO calculations in shower Monte Carlo programs: the POWHEG BOX*, JHEP **06** (2010) 043, arXiv: 1002.2581 [hep-ph] (cit. on p. 5).

[46] P. F. Monni, P. Nason, E. Re, M. Wiesemann and G. Zanderighi, *MiNNLO$_{PS}$: a new method to match NNLO QCD to parton showers*, JHEP **05** (2020) 143, arXiv: 1908.06987 [hep-ph] (cit. on pp. 5, 20).

[47] P. F. Monni, E. Re and M. Wiesemann, *MiNNLO$_{PS}$: optimizing* $2 \to 1$ *hadronic processes*, Eur. Phys. J. C **80** (2020) 1075, arXiv: 2006.04133 [hep-ph] (cit. on p. 5).

[48] J. Isaacson and C. P. Yuan, https://gitlab.com/resbos2/resbos1 (2020) (cit. on p. 6).

[49] J. P. Isaacson, 'ResBos2: Precision Resummation for the LHC Era', PhD thesis: Michigan State U., 2017 (cit. on p. 6).

[50] J. Isaacson, Y. Fu and C. .-P. Yuan, *ResBos2 and the CDF W Mass Measurement*, (2022), arXiv: 2205.02788 [hep-ph] (cit. on pp. 6, 29).

[51] U. Baur, S. Keller and D. Wackeroth, *Electroweak radiative corrections to W boson production in hadronic collisions*, Phys. Rev. D **59** (1999) 013002, arXiv: hep-ph/9807417 (cit. on p. 6).

[52] U. Baur and D. Wackeroth, *Electroweak radiative corrections to* $p\bar{p} \to W^{\pm} \to \ell^{\pm}\nu$ *beyond the pole approximation*, Phys. Rev. D **70** (2004) 073015, arXiv: hep-ph/0405191 (cit. on p. 6).

[53] W. Placzek and S. Jadach, *Multiphoton radiation in leptonic W boson decays*, Eur. Phys. J. C **29** (2003) 325, arXiv: hep-ph/0302065 (cit. on p. 6).

[54] W. Placzek, *WINHAC: The Monte Carlo event generator for single W-boson production in hadronic collisions*, PoS **EPS-HEP2009** (2009) 340, arXiv: 0911.0572 [hep-ph] (cit. on p. 6).

[55] W. Płaczek, S. Jadach and M. W. Krasny, *Drell-Yan processes with WINHAC*, Acta Phys. Polon. B **44** (2013) 2171, arXiv: 1310.5994 [hep-ph] (cit. on p. 6).

[56] C. M. Carloni Calame, G. Montagna, O. Nicrosini and M. Treccani, *Higher order QED corrections to W boson mass determination at hadron colliders*, Phys. Rev. D **69** (2004) 037301, arXiv: hep-ph/0303102 (cit. on p. 6).

[57] C. M. Carloni Calame, G. Montagna, O. Nicrosini and A. Vicini, *Precision electroweak calculation of the charged current Drell-Yan process*, JHEP **12** (2006) 016, arXiv: hep-ph/0609170 (cit. on p. 6).

[58] C. M. Carloni Calame, G. Montagna, O. Nicrosini and A. Vicini, *Precision electroweak calculation of the production of a high transverse-momentum lepton pair at hadron colliders*, JHEP **10** (2007) 109, arXiv: 0710.1722 [hep-ph] (cit. on p. 6).

[59] J. C. Collins and D. E. Soper, *Angular Distribution of Dileptons in High-Energy Hadron Collisions*, Phys. Rev. D **16** (1977) 2219 (cit. on p. 9).

[60] S. Catani and M. Grazzini, *An NNLO subtraction formalism in hadron collisions and its application to Higgs boson production at the LHC*, Phys. Rev. Lett. **98** (2007) 222002, arXiv: hep-ph/0703012 (cit. on p. 9).

[61] S. Catani, L. Cieri, G. Ferrera, D. de Florian and M. Grazzini, *Vector boson production at hadron colliders: a fully exclusive QCD calculation at NNLO*, Phys. Rev. Lett. **103** (2009) 082001, arXiv: 0903.2120 [hep-ph] (cit. on pp. 9, 20).

[62] ATLAS Collaboration, *Measurement of the angular coefficients in Z-boson events using electron and muon pairs from data taken at $\sqrt{s}$ = 8 TeV with the ATLAS detector*, JHEP **08** (2016) 159, arXiv: 1606.00689 [hep-ex] (cit. on pp. 9, 20–22).

[63] CDF and D0 Collaboration, *Combination of CDF and D0 W-Boson Mass Measurements*, Phys. Rev. **D88** (2013) 052018, arXiv: 1307.7627 [hep-ex] (cit. on p. 9).

[64] A. Valassi, *Combining correlated measurements of several different physical quantities*, Nucl. Instrum. Meth. **A500** (2003) 391 (cit. on pp. 10, 33).

[65] D0 Collaboration, *Study of the normalized transverse momentum distribution of W bosons produced in $p\bar{p}$ collisions at $\sqrt{s}$ = 1.96 TeV*, Phys. Rev. D **103** (2021) 012003, arXiv: 2007.13504 [hep-ex] (cit. on p. 14).

[66] B. Efron, *Bootstrap Methods: Another Look at the Jackknife*, The Annals of Statistics **7** (1979) 1, URL: https://doi.org/10.1214/aos/1176344552 (cit. on p. 16).

[67] ATLAS Collaboration, *Electron and photon energy calibration with the ATLAS detector using LHC Run 1 data*, Eur. Phys. J. C **74** (2014) 3071, arXiv: 1407.5063 [hep-ex] (cit. on p. 16).

[68] ATLAS Collaboration, *Measurement of the muon reconstruction performance of the ATLAS detector using 2011 and 2012 LHC proton–proton collision data*, Eur. Phys. J. C **74** (2014) 3130, arXiv: 1407.3935 [hep-ex] (cit. on p. 16).

[69] J. M. Campbell and R. K. Ellis, *MCFM for the Tevatron and the LHC*, Nucl. Phys. B Proc. Suppl. **205-206** (2010) 10, ed. by J. Blümlein, S.-O. Moch and T. Riemann, arXiv: 1007.3492 [hep-ph] (cit. on p. 20).

[70] R. Gavin, Y. Li, F. Petriello and S. Quackenbush, *FEWZ 2.0: A code for hadronic Z production at next-to-next-to-leading order*, Comput. Phys. Commun. **182** (2011) 2388, arXiv: 1011.3540 [hep-ph] (cit. on pp. 20, 34).

[71] J. Bellm et al., *Herwig 7.0/Herwig++ 3.0 release note*, Eur. Phys. J. C **76** (2016) 196, arXiv: 1512.01178 [hep-ph] (cit. on p. 20).

[72] CDF Collaboration, *First Measurement of the Angular Coefficients of Drell-Yan e^+e^- pairs in the Z Mass Region from $p\bar{p}$ Collisions at $\sqrt{s}$ = 1.96 TeV*, Phys. Rev. Lett. **106** (2011) 241801, arXiv: 1103.5699 [hep-ex] (cit. on p. 22).

[73] ATLAS Collaboration, *Measurement of the Z/γ^* boson transverse momentum distribution in pp collisions at $\sqrt{s}$ = 7 TeV with the ATLAS detector*, JHEP **09** (2014) 145, arXiv: 1406.3660 [hep-ex] (cit. on p. 32).

[74] S. Alekhin et al., *HERAFitter*, Eur. Phys. J. C **75** (2015) 304, arXiv: 1410.4412 [hep-ph] (cit. on p. 34).

[75] V. Bertone et al., *xFitter 2.0.0: An Open Source QCD Fit Framework*, PoS **DIS2017** (2018) 203, arXiv: 1709.01151 [hep-ph] (cit. on p. 34).

[76] T. Carli et al., *A posteriori inclusion of parton density functions in NLO QCD final-state calculations at hadron colliders: The APPLGRID Project*, Eur. Phys. J. C **66** (2010) 503, arXiv: 0911.2985 [hep-ph] (cit. on p. 34).

[77] J. M. Campbell and R. K. Ellis, *An Update on vector boson pair production at hadron colliders*, Phys. Rev. **D60** (1999) 113006, arXiv: hep-ph/9905386 [hep-ph] (cit. on p. 34).

[78] Y. Li and F. Petriello, *Combining QCD and electroweak corrections to dilepton production in FEWZ*, Phys. Rev. D **86** (2012) 094034, arXiv: 1208.5967 [hep-ph] (cit. on p. 34).

[79] A. Arbuzov et al., *One-loop corrections to the Drell-Yan process in SANC. I. The Charged current case*, Eur. Phys. J. C **46** (2006) 407, [Erratum: Eur.Phys.J.C 50, 505 (2007)], arXiv: hep-ph/0506110 (cit. on p. 34).

[80] A. Arbuzov et al., *One-loop corrections to the Drell–Yan process in SANC. (II). The Neutral current case*, Eur. Phys. J. C **54** (2008) 451, arXiv: 0711.0625 [hep-ph] (cit. on p. 34).

[81] A. Arbuzov et al., *Update of the MCSANC Monte Carlo integrator, v. 1.20*, JETP Lett. **103** (2016) 131, arXiv: 1509.03052 [hep-ph] (cit. on p. 34).

[82] CDF Collaboration, *Direct Measurement of the W Production Charge Asymmetry in $p\bar{p}$ Collisions at $\sqrt{s}$ = 1.96 TeV*, Phys. Rev. Lett. **102** (2009) 181801, arXiv: 0901.2169 [hep-ex] (cit. on p. 34).

[83] CDF Collaboration, *Measurement of $d\sigma/dy$ of Drell-Yan e^+e^- pairs in the Z Mass Region from $p\bar{p}$ Collisions at $\sqrt{s}$ = 1.96 TeV*, Phys. Lett. B **692** (2010) 232, arXiv: 0908.3914 [hep-ex] (cit. on p. 34).

[84] D0 Collaboration, *Measurement of the Shape of the Boson Rapidity Distribution for $p\bar{p} \to Z/\gamma^* \to e^+e^- + X$ Events Produced at $\sqrt{s}$ of 1.96-TeV*, Phys. Rev. D **76** (2007) 012003, arXiv: hep-ex/0702025 (cit. on p. 34).

[85] D0 Collaboration, *Measurement of the Muon Charge Asymmetry in $p\bar{p} \to W+X \to \mu\nu + X$ Events at $\sqrt{s}$=1.96 TeV*, Phys. Rev. D **88** (2013) 091102, arXiv: 1309.2591 [hep-ex] (cit. on p. 34).

[86] D0 Collaboration, *Measurement of the electron charge asymmetry in $\boldsymbol{p\bar{p} \to W + X \to e\nu + X}$ decays in $\boldsymbol{p\bar{p}}$ collisions at $\boldsymbol{\sqrt{s} = 1.96}$ TeV*, Phys. Rev. D **91** (2015) 032007, [Erratum: Phys.Rev.D 91, 079901 (2015)], arXiv: 1412.2862 [hep-ex] (cit. on p. 34).

[87] ATLAS Collaboration, *Precision measurement and interpretation of inclusive W^+, W^- and Z/γ^* production cross sections with the ATLAS detector*, Eur. Phys. J. C **77** (2017) 367, arXiv: 1612.03016 [hep-ex] (cit. on p. 34).

[88] H1 Collaboration, *Inclusive Deep Inelastic Scattering at High Q^2 with Longitudinally Polarised Lepton Beams at HERA*, JHEP **09** (2012) 061, arXiv: 1206.7007 [hep-ex] (cit. on p. 42).

[89] G. P. Salam and E. Slade, *Cuts for two-body decays at colliders*, JHEP **11** (2021) 220, arXiv: 2106.08329 [hep-ph] (cit. on p. 42).

[90] S. Alekhin, A. Kardos, S. Moch and Z. Trócsányi, *Precision studies for Drell–Yan processes at NNLO*, Eur. Phys. J. C **81** (2021) 573, arXiv: 2104.02400 [hep-ph] (cit. on p. 42).